Deficiency in hematopoietic phosphatase Ptpn6/Shp1 hyperactivates the innate immune system and impairs control of bacterial infections in zebrafish embryos

Kanwal, Z.; Zakrzewska, A.; Hertog, J. den; Spaink, H.P.; Schaaf, M.J.; Meijer, A.H.

The Journal of Immunology

RESEARCH ARTICLE | FEBRUARY 15 2013

Deficiency in Hematopoietic Phosphatase Ptpn6/Shp1 Hyperactivates the Innate Immune System and Impairs Control of Bacterial Infections in Zebrafish Embryos

Zakia Kanwal; ... et. al

J Immunol (2013) 190 (4): 1631–1645.
https://doi.org/10.4049/jimmunol.1200551

Deficiency in Hematopoietic Phosphatase Ptpn6/Shp1 Hyperactivates the Innate Immune System and Impairs Control of Bacterial Infections in Zebrafish Embryos

Zakia Kanwal,* Anna Zakrzewska,* Jeroen den Hertog,*,† Herman P. Spaink,* Marcel J. M. Schaaf,* and Annemarie H. Meijer*

Deficiency in Src homology region 2 domain-containing phosphatase 1/protein tyrosine phosphatase nonreceptor type 6 (SHP1/PTPN6) is linked with chronic inflammatory diseases and hematological malignancies in humans. In this study, we exploited the embryonic and larval stages of zebrafish (*Danio rerio*) as an animal model to study *ptpn6* function in the sole context of innate immunity. We show that *ptpn6* knockdown induces a spontaneous inflammation-associated phenotype at the late larval stage. Surprisingly, glucocorticoid treatment did not suppress inflammation under *ptpn6* knockdown conditions but further enhanced leukocyte infiltration and proinflammatory gene expression. Experiments in a germ-free environment showed that the late larval phenotype was microbe independent. When *ptpn6* knockdown embryos were challenged with *Salmonella typhimurium* or *Mycobacterium marinum* at earlier stages of development, the innate immune system was hyperactivated to a contraproductive level that impaired the control of these pathogenic bacteria. Transcriptome analysis demonstrated that Kyoto Encyclopedia of Genes and Genomes pathways related to pathogen recognition and cytokine signaling were significantly enriched under these conditions, suggesting that *ptpn6* functions as a negative regulator that imposes a tight control over the level of innate immune response activation during infection. In contrast to the hyperinduction of proinflammatory cytokine genes under *ptpn6* knockdown conditions, anti-inflammatory *il10* expression was not hyperinduced. These results support that *ptpn6* has a crucial regulatory function in preventing host-detrimental effects of inflammation and is essential for a successful defense mechanism against invading microbes. ***The Journal of Immunology*****, 2013, 190: 1631–1645.**

The innate immune system has been conserved in evolution from invertebrate to vertebrate organisms and plays an indispensable role in host protection against infections. The vertebrate innate immune system has been demonstrated to not only function as the first line of defense against microorganisms, but also to be required for activating the secondary adaptive defenses. However, if the innate immune system goes unchecked, the production of inflammatory mediators can cause considerable tissue damage. Recent studies indicate that defects in the initial sensing of microorganisms and allergens by the innate immune system can contribute to autoimmune and autoinflammatory diseases, which were classically viewed as specific disorders of the adaptive immune system (1–3). In healthy individuals, the innate immune response is tightly controlled by complex regulatory mechanisms that prevent excessive and chronic inflammation (4). The Src homology region 2 domain-containing phosphatase 1 (SHP1), encoded by the *PTPN6* gene, has been recognized as a critical factor in this process of negative regulation.

SHP1 belongs to the family of protein tyrosine phosphatases (PTPs), which dephosphorylate phosphotyrosyl residues in proteins that are phosphorylated by protein tyrosine kinases. PTPs and protein tyrosine kinases function in a variety of cellular processes, from cell survival to proliferation, differentiation, migration, and immune responses. SHP1 (PTPN6) and SHP2 (PTPN11) are closely related non–receptor-type PTPs, each having two Src homology 2 domains N-terminal to the phosphatase catalytic domain (5–7). Although SHP2 is expressed ubiquitously, SHP1 is predominantly expressed in hematopoietic cell lineages, and it has been implicated in the regulation of a diverse range of cytokine receptors, growth factor receptors, and immunoreceptors (5, 6, 8). SHP1 has been shown to associate with ITIMs in these receptors (5, 6) and has been proposed to bind to ITIM-like motifs in various kinases, including IL-1R–associated kinase 1, ERK1/2, p38, JNK, JAK2, JAK3, TAK1, IκB kinase α, and LYN (9, 10).

SHP1 has been extensively studied after the discovery of two naturally occurring mutant mouse strains: motheaten (*me*), considered to carry a null allele of the *Ptpn6* gene, and motheaten viable (*mev*), which encodes a phosphatase with ~20% of wild-type

*Institute of Biology, Leiden University, 2333 CC Leiden, The Netherlands; and †Hubrecht Institute–Koninklijke Nederlandse Akademie van Wetenschappen and University Medical Center Utrecht, 3584 CT Utrecht, The Netherlands

Received for publication February 15, 2012. Accepted for publication December 11, 2012.

This work was supported by the SmartMix Programme of the Netherlands Ministry of Economic Affairs and the Ministry of Education, Culture and Science and by the European Commission 6th and 7th Framework projects High-throughput Tools for Biomedical Screens in Zebrafish (LSHG-2006-037220) and Zebrafish Regulomics for Human Health (HEALTH-F4-2010-242048). Z.K. was supported by the Higher Education Commission of Pakistan. A.Z. was supported by a Horizon grant of the Netherlands Genomics Initiative.

The microarray data presented in this article have been submitted to the Gene Expression Omnibus (http://www.ncbi.nlm.nih.gov/geo/query/acc.cgi?acc=GSE34930) under accession number GSE34930.

Address correspondence and reprint requests to Dr. Annemarie H. Meijer, Institute of Biology, Leiden University, Einsteinweg 55, 2333 CC Leiden, The Netherlands. E-mail address: a.h.meijer@biology.leidenuniv.nl

Abbreviations used in this article: dpf, days postfertilization; dpi, days postinfection; GR, glucocorticoid receptor; GZM, gnotobiotic zebrafish medium; hpf, hours post fertilization; hpi, hours postinfection; KEGG, Kyoto Encyclopedia of Genes and Genomes; Mmp, matrix metalloproteinase; MO, morpholino; Mpx, myeloperoxidase; NA, numerical aperture; PTP, protein-tyrosine phosphatase; qPCR, quantitative RT-PCR; RT-MLPA, reverse transcription–multiplex ligation–dependent probe amplification; SHP1, Src homology region 2 domain-containing phosphatase 1; WISH, whole-mount in situ hybridization.

catalytic activity (11–13). These mice suffer from severe immune disorders, with spontaneous inflammatory activity affecting multiple organs, including the lungs, kidney, joints, and skin, the latter resulting in their typical motheaten appearance. The mutations result in lethal pneumonitis by 3 (*me*) or 9 (*mev*) wk of age. Backcrossing of *mev* mice to *rag1* null mutants (that do not contain mature T and B cells) did not alleviate the *motheaten* inflammatory disease, indicating that the function of myeloid cells rather than the function of the adaptive immune system is required for major aspects of the *shp1* mutant phenotype (14). Furthermore, pulmonary inflammation in *mev* mutants was found to depend strongly on the function of mast cells (15). A viable hypomorphic allele of *Ptpn6*, *spin* (spontaneous inflammation), carrying a point mutation in one of the Src homology 2 domains, was later described that elicits chronic inflammatory and autoimmune disease (16). Inflammation in *spin* mutants was triggered by the presence of microbes and found dependent on production of IL-1, subsequent IL-1 signaling, and the presence of neutrophils (16, 17). Consistent with these findings, SHP1 was shown to negatively regulate TLR-mediated production of proinflammatory cytokines by suppressing the activation of MAPKs and the transcription factor NF-κB (18).

SHP1 has been associated with several human inflammatory diseases. In patients with psoriatic inflammatory skin disease, deficient SHP1 expression in T cells has been observed (19). Furthermore, macrophages of multiple sclerosis patients display SHP1 deficiency concomitant with enhanced expression of genes mediating inflammatory demyelination in multiple sclerosis pathogenesis (20). Finally, it has been suggested that altered expression of SHP1 may also be associated with human allergies and asthmatic disease based on recent studies in mice that indicate a role of SHP1 in mast cells and allergic inflammatory responses (21). In addition, SHP1 is considered a putative tumor suppressor. Decreased expression of SHP1 has been observed in many types of human lymphomas and leukemias. The reduced levels of SHP1 in these malignancies have been attributed to mutations, epigenetic regulation, and posttranscriptional mechanisms (22, 23). SHP1 has also been implicated as a negative regulator of insulin signaling and clearance of insulin in the liver and has been linked to progression of diabetic retinopathy (24, 25).

As many recent studies have shown, the zebrafish embryo model has specific advantages not only for developmental biology but also for studying immunity, inflammation, and infections (26–28). The embryo model is particularly useful for studying responses of the innate immune system, as macrophages and neutrophils develop during the first 2 d of embryogenesis, when the adaptive immune system is not yet in place (29). The zebrafish genome encodes orthologs of the majority of human PTPs, including *shp1/ptpn6* and *shp2/ptpn11a* (30). We have previously shown that hematopoietic expression of *shp1/ptpn6* is conserved in zebrafish embryos and controlled by the transcription factor Pu.1 (Spi1), like its human counterpart (31, 32). The zebrafish embryo model was also exploited to study the role of *shp2* in early development and to investigate the cell biological effects of activating and inactivating mutations in Shp2 protein that underlie the Noonan and LEOPARD syndromes in humans. Defective Shp2 signaling induced cell movement defects as early as gastrulation and zebrafish embryos expressing Noonan or LEOPARD Shp2 displayed craniofacial and cardiac defects, reminiscent of human symptoms (33).

In this study, we used morpholino knockdown to study the effect of *ptpn6* deficiency in zebrafish embryos. No visible phenotypic effects of *ptpn6* knockdown were observed during early development, but morphant larvae developed a late phenotype at 5 to 6 d postfertilization (dpf). Skin lesions in these morphants were reminiscent of phenotypes of the murine *Ptpn6* mutants, *motheaten* and *spin,* which suffer from severe inflammation leading to patches of hair loss and foot lesions, as discussed above (12, 16). Based on leukocyte infiltration and proinflammatory gene expression, we concluded that also the zebrafish *ptpn6* morphant phenotype is associated with an inflammatory response. We describe infection experiments of *ptpn6* morphants with bacterial pathogens at 1 dpf, which is several days prior to the manifestation of the late inflammation-associated phenotype. We observed that *ptpn6* morphants responded to bacterial challenge with increased induction of proinflammatory genes compared with wild-type embryos, yet their ability to control these infections was severely impaired, indicating that this is not a functional response. In conclusion, our data support the role of *ptpn6* as a negative regulator of the innate immune system, which is important for a functional innate immune response during bacterial infections.

Materials and Methods

Zebrafish husbandry

Zebrafish were handled in compliance with the local animal welfare regulations and maintained according to standard protocols (http://zfin.org). Zebrafish lines used in this study included AB/TL, *tp53*^{M214K} (34), *Tg(mpx:GFP)i114* (35), *Tg(fli1:EGFP)* (36) and *Tg(-1.0pomca:GFP)zf44;Tg(prl:RFP)zf113* (37). Embryos were grown at 28.5–30°C in egg water (60 μg/ml Instant Ocean sea salts). For the duration of bacterial injections, embryos were kept under anesthesia in egg water containing 200 μg/ml tricaine (Sigma-Aldrich). Embryos used for whole-mount in situ hybridization (WISH) and immunostaining were kept in egg water containing 0.003% 1-phenyl-2-thiourea (Sigma-Aldrich) to prevent melanization.

Morpholino knockdown

Morpholino oligonucleotides (Gene Tools) were diluted to the desired concentration in 1× Danieau buffer [58 mM NaCl, 0.7 mM KCl, 0.4 mM $MgSO_4$, 0.6 mM $Ca(NO_3)_2$, 5.0 mM HEPES (pH 7.6)] containing 1% phenol red (Sigma-Aldrich), and ~1 nL was injected at the 1 to 2 cell stage using a Femtojet injector (Eppendorf). For knockdown of *ptpn6*, three morpholinos (MOs) were used that specifically target *ptpn6* and do not match with the related *ptpn11* (*shp2*) phosphatase or other genes: MO1 (5′-ACTCATTCCTTACCCGATGCGGAGC-3′; 0.06 mM) targets the exon 11/intron 11 to 12 splice junction resulting in deletion of exon 11; MO2 (5′-CTGTGAAACCACCGAACCATCTTCC-3′; 0.20 mM) targets the translation start site; and MO3 (5′-TGTTCTGTTGGCATACAGAAACAGA-3′; 0.08 mM) targets the exon 9/intron 9 to 10 splice junction, resulting in insertion of introns 9 and 10. Splice-blocking MO effects (Supplemental Fig. 1A, 1B) were verified by sequencing of RT-PCR products. As a control, we used the standard control MO from GeneTools at the same concentrations as the *ptpn6* MOs.

WISH, immunodetection, TUNEL assay, and myeloperoxidase activity assay

For all assays, embryos were fixed in 4% paraformaldehyde in PBS. WISH using alkaline phosphatase detection with BM Purple substrate (Roche Diagnostics) was carried out as previously described (38). Digoxigenin-labeled *mfap4* and *mpx* probes were generated as described in Zakrzewska et al. (31). Immunofluorescence stainings were performed with 1:500 dilutions of polyclonal rabbit Ab against phospho-histone H3 (Santa Cruz Biotechnology) and L-plastin (39). For detection, Alexa Fluor 568/488 goat anti-rabbit IgG secondary Ab (Molecular Probes) as described in Cui et al. (40) were used. DNA fragmentation during apoptotic cell death was examined by TUNEL using the ApopTag Peroxidase In Situ Apoptosis Detection Kit (Millipore) according to the manufacturer's instructions. Embryos were fixed, permeabilized, treated with proteinase K, and refixed in 4% paraformaldehyde as for WISH. Embryos were then fixed in ethanol/acetic acid 2:1 for 15 min at −20°C followed by PBS washes. After 15 min incubation in the equilibration buffer, embryos were transferred to working-strength TdT enzyme solution supplemented with 0.3% Triton X-100 and incubated for 1 h on ice followed by 1 h at 37°C. The reaction was stopped by a 5-min wash in stop solution at room temperature, followed by 45 min incubation at 37°C and PBS washes. Subsequent immunodetection with alkaline phosphatase–conjugated anti-DIG Fab fragments and BM purple staining was performed as for WISH. Histochemical staining for

myeloperoxidase (Mpx) activity was performed with the Peroxidase Leukocyte Kit (Sigma-Aldrich) as described in Cui et al. (40).

RNA isolation, quantitative RT-PCR, and reverse transcription–multiplex ligation–dependent probe amplification

RNA isolation and quantitative RT-PCR (qPCR) analysis was performed as described in Stockhammer et al. (38). Primer sequences for *ppial*, *il1b*, *mmp9*, *lgals*, *mpeg1*, *cxcr3.2*, *mfap4*, and *marco* are described in Zakrzewska et al. (31) and Stockhammer et al. (38). Additional primer sequences used were: *lyz*, forward 5′-TGTCCTCGTGTGAAAGCAAGAC-3′ and reverse 5′-AGAATCCCTCAAATCCATCAAGCC-3′; *mpx*, forward 5′-AAGACA-ATGCACGAGAGC-3′ and reverse 5′-GCAATGAAGCAAGGAACC-3′; *csf1r*, forward 5′-CTGCTGGTCGTAGAGGAG-3′ and reverse 5′-TGTGA-AGTCAGAGGAGG-3′; and *ncf1*, forward 5′-CACAGGATGGCTGAAA-CATACG-3′ and reverse 5′-TAGTGCTGGCTGGGAAAGAATC-3′.

Reverse transcription–multiplex ligation–dependent probe amplification (RT-MLPA) was performed as described in Rotman et al. (41).

Germ-free experiments

For generating germ-free embryos, we used a natural breeding method described in Pham et al. (42). Eggs were washed three times in antibiotic gnotobiotic zebrafish medium (GZM) prior to performing MO injections in a downflow cabinet using sterilized needles and equipment. Following injections, eggs were immediately washed with antibiotic GZM and successively treated with povidone-iodide and bleach solutions, as described (42). Embryos were grown in six-well plates at 28°C wrapped in aluminum foil, and sterile antibiotic GZM was refreshed daily. At the end of the experiment, sterility was tested by plating media from the germ-free and conventionally raised embryos on tryptic soy agar plates.

Chemical treatments

Betamethasone 17-valerate (1 μM), beclomethasone (25 μM), and prednisolone (25 μM) were dissolved in 0.1% DMSO and added directly to egg water at 1 or 3 dpf; solutions were refreshed daily. Concentrations used were based on EC_{50} in cell-culture experiments. Controls were treated with DMSO only. $CuSO_4$-induced inflammation was performed as in d'Alençon et al. (43). Matrix metalloproteinase (Mmp) inhibitors MMP-2/MMP-9 inhibitor V (Calbiochem; 2 μM) and GM6001 MMP inhibitor (Millipore; 25 μM) were dissolved in DMSO and added directly to egg water at 1 dpf; solutions were refreshed daily. Controls were treated with DMSO only.

Infection experiments

Salmonella typhimurium infections were performed using the *S. typhimurium* strain SL1027 and its isogenic LPS Ra mutant derivative SF1592, carrying the DsRed expression vector pGMDs3 (44). For *Mycobacterium marinum* infection experiments, the Mma20 strain was used expressing mCherry in the pSMT3 vector (45). Bacteria were grown and prepared for injections as described in Cui et al. (40) and microinjected into the caudal vein of embryos at 28 h postfertilization (hpf) using a dose of 200–250 CFUs *S. typhimurium* or 100 CFUs *M. marinum* per embryo. After injections, embryos were transferred to fresh egg water and incubated at 28°C. For plating assays, infected embryos were homogenized using a Retsch mixer mill with a metal bead for 1 min at maximum speed.

Microarray analysis

For microarray analysis of *S. typhimurium* infection in *ptpn6* morphants, three independent infection experiments were performed. In each experiment, RNA was isolated from pools of 15–20 embryos per treatment group. Knockdown of *ptpn6* was performed using MO1, and control embryos were injected with Danieau buffer/phenol red. The *ptpn6* morphants and control embryos were infected at 28 hpf with *S. typhimurium* SL1027 bacteria or mock-injected with PBS as a control. RNA extraction was performed at 8 h postinfection (hpi). Microarray analysis was performed using a previously described custom-designed 44K Agilent chip (Agilent Technologies) (38). All RNA samples were labeled with Cy5 and hybridized against a Cy3-labeled common reference, which consisted of a mixture of all samples from the infection study. Labeling, hybridization, and data analysis using Rosetta Resolver 7.0 was performed as previously described (38). The raw data were submitted to the Gene Expression Omnibus database under accession number GSE34930. Kyoto Encyclopedia of Genes and Genomes (KEGG) pathway analysis was performed using DAVID v6.7 (http://david.abcc.ncifcrf.gov/home.jsp) (46).

Microscopy and image analysis

Bright-field images of embryos were obtained with a Leica M165C stereomicroscope equipped with a DFC420C digital color camera (Leica Microsystems) (Figs. 1, 2A, 2B, 2G, 2H, 3E –H, Supplemental Fig. 1G–L). Composite images of different focal planes were created with Adobe Photoshop (Adobe Systems). Fluorescence images were taken with a Leica MZ16FA stereo fluorescence microscope equipped with a DFC420C digital color camera (Leica Microsystems) (Figs. 2C–F, 2I–L, 3A, 3B, 3I–L, 5C–F, 5H–M, Supplemental Fig. 1C–F, 1M–O). Overlay images of bright-field and fluorescence stereomicroscopy were made in Adobe Photoshop (Adobe Systems). Confocal microscopy was performed with a Leica TCS SPE confocal microscope (Leica Microsystems) (Fig. 3C, 3D: HC PLAN APO objective 20×/0.70 numerical aperture (NA); Fig. 4K: HCX APO objective 40×/0.80 NA; Fig. 5N–Q) or Zeiss LSM5 Exciter system (Carl Zeiss) (Fig. 4A–F: APO objective 10×/0.3 NA). Maximum intensity projections of Z-stacks of different focal planes were obtained using Image J (National Institutes of Health). Pixel counts on stereo fluorescence images were performed as described in Stoop et al. (47).

Results

Knockdown of ptpn6 *causes a late phenotype in zebrafish larvae that is characterized by enhanced proliferation, apoptosis, and inflammation*

To study the function of the *ptpn6* gene in zebrafish, a knockdown study of this gene was performed using a splice-blocking MO (MO1) that causes deletion of the phosphatase catalytic domain. MO knockdown did not have strong effects on embryo morphology at 1–3 dpf, except that the heads and eyes of *ptpn6* morphants were slightly smaller compared with the controls (Figs. 1A, 1B, 1H, 1I, 2). Furthermore, L-plastin immunostaining, in situ hybridization with *mfap4* and *mpx* markers, and Mpx activity assays demonstrated that macrophage and neutrophil numbers and the migratory responses of these cells toward injury were normal (Fig. 2).

However, at later stages of development, pleiotropic effects on larval morphology were observed that became progressively severe. At 3 dpf, some embryos showed a minor edema of the heart cavity (Fig. 1B, 1I), which became more prominent at 4 dpf (Fig. 1C, 1J). At 5 to 6 dpf, 80–90% of morphant larvae additionally developed lesions on the eyes and skin, and in severe cases, they also developed edema between the trunk and the yolk sac and yolk extension (Fig. 1D–G, 1K–N). The heart beat frequency was unaffected in *ptpn6* morphants until 4 dpf, but was ∼40% reduced in larvae of 6 dpf, as the likely result of the increased cardiac edema at this stage (data not shown). MO injection of *Tg(fli1:EGFP)* embryos did not reveal defects in vascular development (Supplemental Fig. 1C–F).

Because mammalian *ptpn6*/*shp1* has been implicated in negative regulation of growth factor, MAPK, and NF-κB signaling pathways, we investigated proliferation, apoptosis, and inflammation in *ptpn6* morphants. Phosphohistone H3 immunolabeling revealed increased numbers of mitotic cells in *ptpn6* morphants in a specific region on the dorsal side of the brain and in the retina at 5 dpf (Fig. 3A–D). Furthermore, increased numbers of apoptotic cells were detected with a TUNEL assay, particularly in the brain and the region of cardiac edema at this stage (Fig. 3E–H). To determine if the phenotype of the zebrafish *ptpn6* morphants was associated with inflammation, we performed immunofluorescence staining using anti–L-plastin Ab, which stains all leukocytes (39). The results showed that leukocytes in 5 dpf *ptpn6* morphants accumulated around the edemic area of the heart cavity and at skin lesions, whereas they had largely disappeared from their normal location in the caudal hematopoietic tissue (Fig. 3I–L). In addition, we checked the expression of the proinflammatory genes *il1b* and *mmp9*. qPCR showed that, concomitant with the appearance of the strong phe-

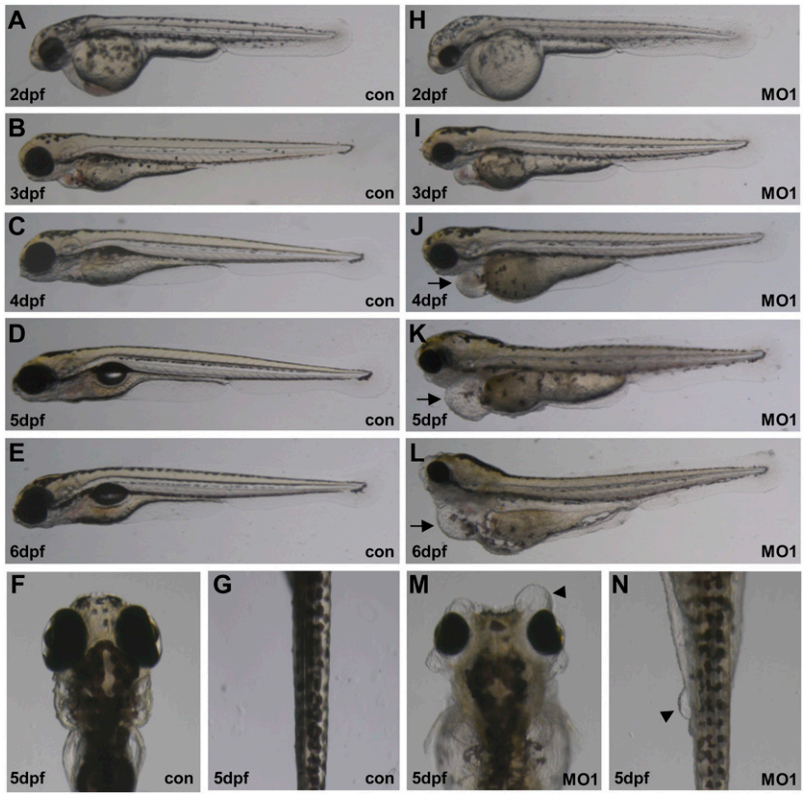

FIGURE 1. Late pleiotropic phenotype in *ptpn6* morphant zebrafish larvae. (**A**–**G**) Embryos injected with standard control morpholino (con). (**H**–**N**) embryos injected with *ptpn6* MO (MO1). Phenotypes are shown at 2–6 dpf in lateral [(A–E), (H–L), anterior to the *left*] or dorsal view [(F), (G), (M), (N), anterior to the *top*]. Dorsal views show head and trunk (F, M) or the tail region (G, N). Skin lesions in *ptpn6* morphants are indicated with arrowheads, and cardiac edema is indicated with arrows.

notypic defects at 5 to 6 dpf, the expression levels of *il1b* and *mmp9* were enhanced in *ptpn6* morphant embryos compared with the controls at 5 and 6 dpf, but not at 4 dpf (Fig. 3M, 3P). We conclude, based on leukocyte infiltration and enhanced *il1b* and *mmp9* expression, that the late pleiotropic phenotype of *ptpn6* morphant larvae is associated with inflammation.

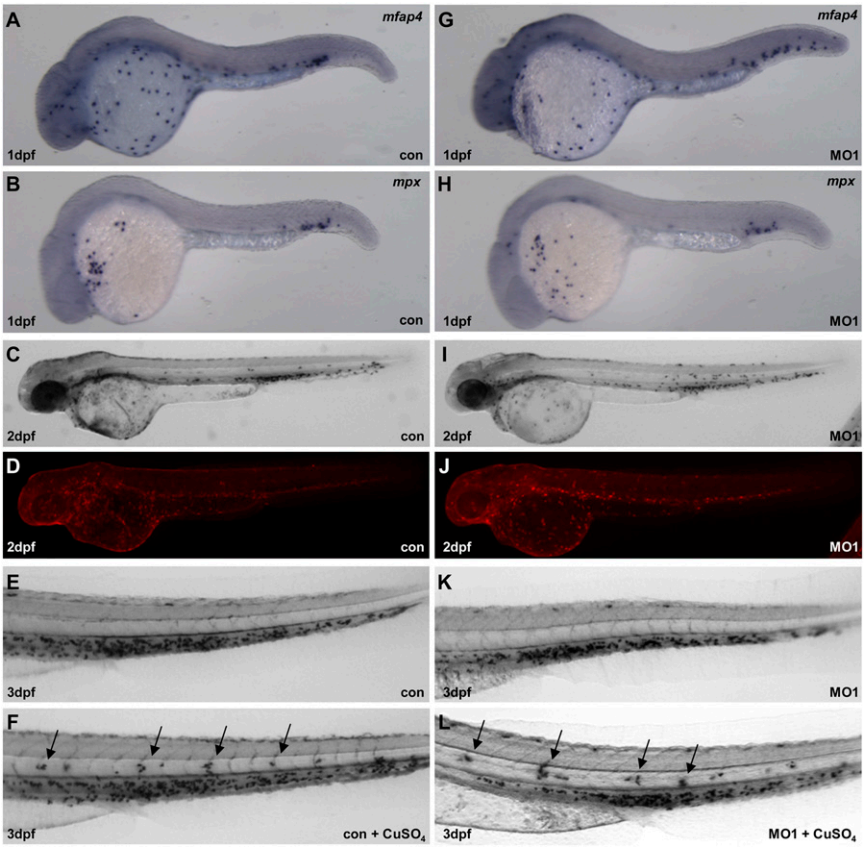

FIGURE 2. Unaltered leukocyte development and migratory response in *ptpn6* morphants. (**A**–**F**) Embryos injected with standard control MO (con). (**G**–**L**) Embryos injected with *ptpn6* MO (MO1). (A and G) In situ hybridization with macrophage marker *mfap4* (31) at 1 dpf. (B and H) In situ hybridization with neutrophil marker *mpx* at 1 dpf. (C and I) Histochemical staining for Mpx enzyme activity at 2 to 3 dpf. (D and J) Immunolabeling of the same embryos as in (C) and (I) with Ab against the general leukocyte marker L-plastin and staining with AlexaFluor 568 anti-rabbit IgG secondary Ab. (E, F, K, and L) Histochemical staining for Mpx enzyme activity in larvae incubated for 2 h with (F, L) or without (E, K) 10 μM $CuSO_4$ at 3 dpf. Chemically induced inflammation by $CuSO_4$ treatment (43) is due to damage of hair cells of the lateral line neuromasts, which attracts neutrophils (arrows in F, L). Embryos are shown in lateral view with the anterior to the *left*. The images are representative examples of ≥20 larvae in each group.

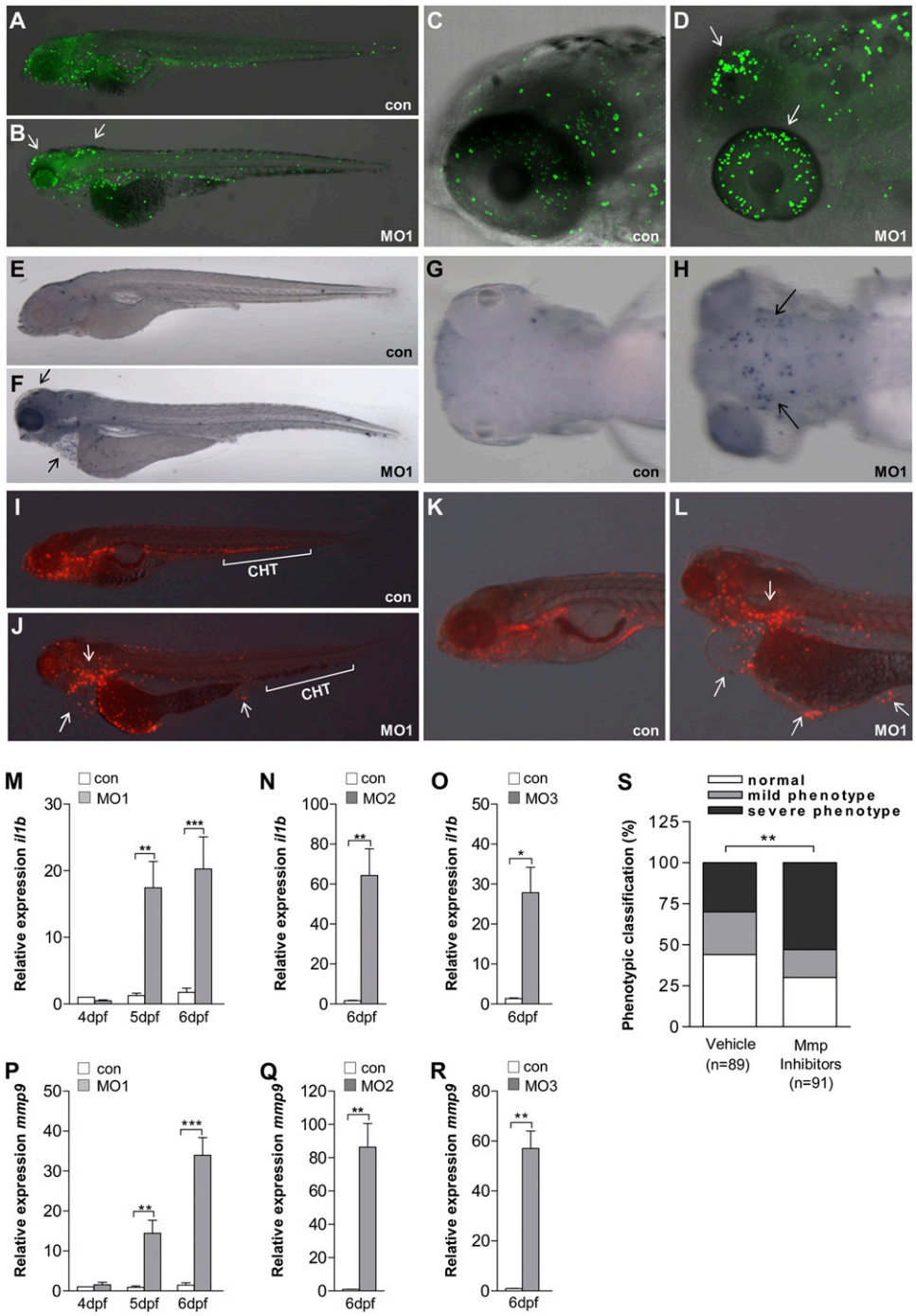

FIGURE 3. Enhanced proliferation, apoptosis, and inflammation in *ptpn6* morphants. (**A**–**D**) Phosphohistone H3 immunolabeling with AlexaFluor 488 anti-rabbit IgG secondary Ab staining. (**E**–**H**) TUNEL assay. (**I**–**L**) Immunolabeling with Ab against the general leukocyte marker L-plastin and staining with AlexaFluor 568 anti-rabbit IgG secondary Ab. Embryos were injected with standard control (con) or *ptpn6* (MO1) MOs, and all assays were performed at 5 dpf. Larvae or head details are shown in lateral (A–D, E, F, I–L) or dorsal (G, H) view with the anterior to the *left*. Stereo microscope images (A, B, E–L) and confocal Z-stack projections (C, D, transmitted light and fluorescence overlay) are representative examples of ≥20 larvae in each group. Arrows indicate regions with increased numbers of proliferating cells (B, D), increased numbers of apoptotic cells (F, H), and accumulation of leukocytes around sites of cardiac edema and skin lesions (J, L) in *ptpn6* morphants. Also note the absence of immune cells in the caudal hematopoietic tissue (CHT) of *ptpn6* morphants (J) compared with the control (I). (**M**–**R**) Increased expression of proinflammatory genes in *ptpn6* morphants. Embryos were injected with splice-blocking (MO1, MO3) or translation-blocking (MO2) MOs targeting *ptpn6* or with standard control MO (con). RNA was isolated at 4–6 dpf from pools of 10–20 larvae, which were picked randomly in the case of con, MO1, and MO3 MO injections. In the case of MO2, which has a lower penetrance, 10–20 larvae showing the edema and skin lesion phenotype were selected. Gene expression levels of *il1b* (M–O) and *mmp9* (P–R) were determined by qPCR, and relative expression levels are shown. In the 4–6 dpf time course (M, P), the 4 dpi control group is set at 1. Data are the mean ± SEM of three independent experiments. Asterisks indicate significant differences tested by two-way ANOVA analysis with Bonferroni method as post hoc test (M, P) or with an unpaired *t* test (N, O, Q, R). (**S**) Rescue of the *ptpn6* MO effect by Mmp inhibitors. Embryos injected with MO1 were treated with 25 μM MMP inhibitor GM6001 and 2 μM MMP-2/MMP-9 inhibitor V (in DMSO) or vehicle (DMSO) from 1 until 5 dpf, after which phenotypes were scored. Embryos were classified as normal (no morphological abnormalities), mild phenotype (cardiac edema), or severe phenotype (cardiac edema, edema between the trunk and the yolk sac/yolk extension, and skin lesions). Phenotypic classification data were accumulated from three independent experiments. The difference between vehicle and Mmp inhibitor treatment was significant by a χ^2 test. $^*p < 0.05$, $^{**}p < 0.01$, $^{***}p < 0.001$.

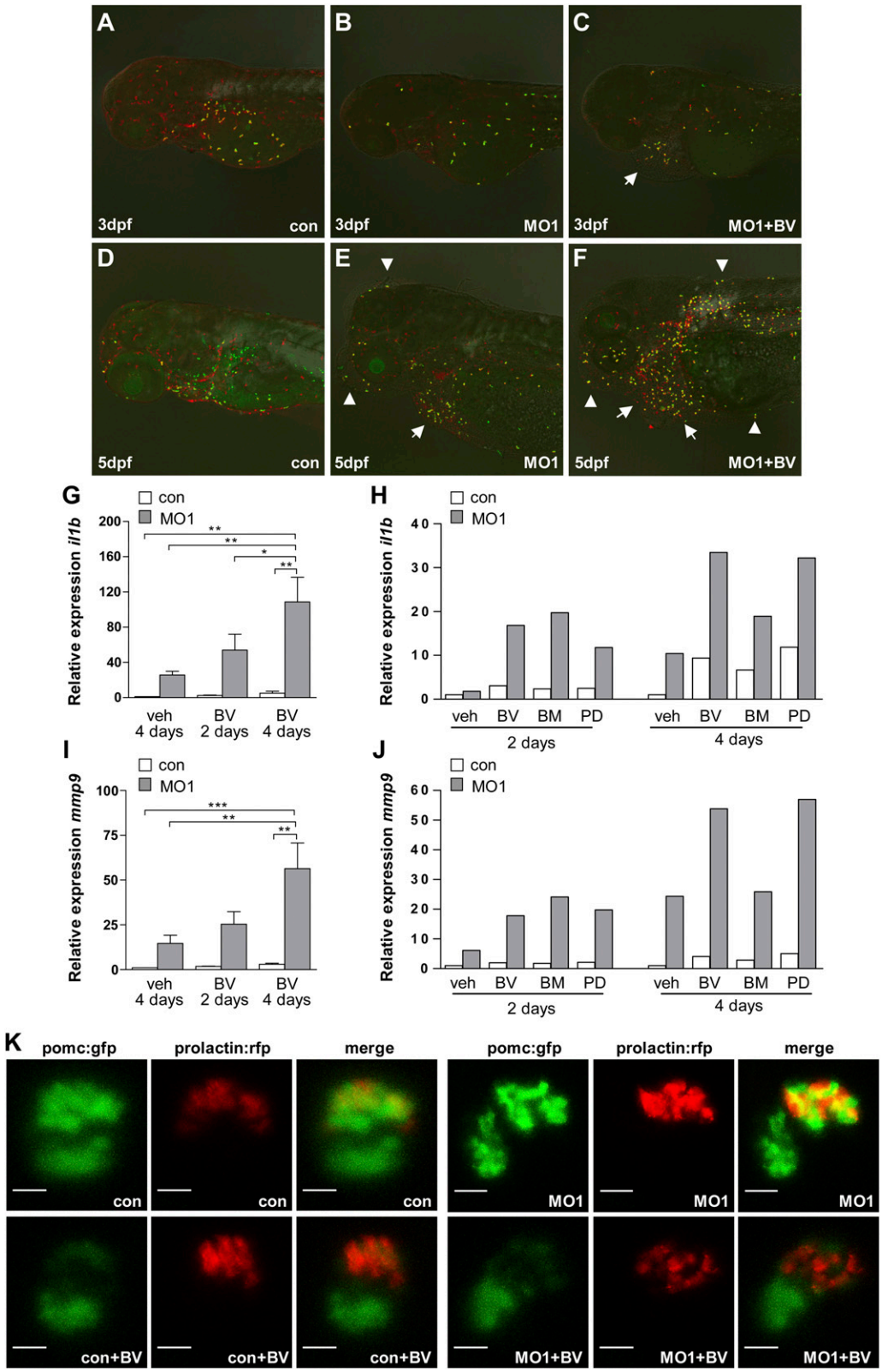

FIGURE 4. Enhanced leukocyte infiltration and inflammatory gene expression by glucocorticoid treatment of *ptpn6* morphants. (**A**–**F**) Embryos of the *Tg (mpx:GFP)i114* neutrophil marker line were injected with standard control (con) or *ptpn6* (MO1) MO and treated at 1 dpf with 1 μM betamethasone 17-valerate (BV) in 0.1% DMSO or with 0.1% DMSO as a control. Immunolabeling with Ab against the general leukocyte marker L-plastin and staining with AlexaFluor 568 anti-rabbit IgG secondary Ab was performed at 3 and 5 dpf. Confocal Z-stacks (fluorescence and transmission overlay) of the larval heads (lateral view, anterior to the *left*, original size ~2 mm) are representative examples of ≥20 larvae in each group. Accumulation of leukocytes around sites of cardiac edema and skin lesions in *ptpn6* morphants is indicated with arrows and arrowheads, respectively. (**G**–**J**) Embryos were injected with standard control (con) or *ptpn6* (MO1) MO and treated with BV, beclomethasone (BM), prednisolone (PD), or vehicle (veh; 0.1% DMSO) for 2 d starting at 3 dpf or for 4 d starting at 1 dpf, as indicated. RNA was isolated at 5 dpf from pools of 10–20 larvae. Gene expression levels of *il1b* (G, H) and *mmp9* (I, J) were determined by qPCR, and relative expression levels are shown with the untreated control group set at 1. Data in (G) and (I) are the (*Figure legend continues*)

The ptpn6 *morphant phenotype is phenocopied with different MOs and partially rescued with Mmp inhibitors*

Attempts to rescue the MO1 phenotype by *ptpn6* mRNA coinjection were unsuccessful, because ectopic overexpression caused aberrant development at 1 dpf. However, the MO1 knockdown effect could be phenocopied with two additional MOs, a translation-blocking MO (MO2) and a splice-blocking MO (MO3) introducing a stop codon in the phosphatase catalytic domain due to intron insertion. After injection with MO3, between 50 and 60% of the larvae at 5 to 6 dpf showed similar phenotypic abnormalities as with MO1, whereas the effect of MO2 injection had a lower penetrance, with 5–10% of larvae displaying severe edema and skin lesions (Supplemental Fig. 1G–I). Expression levels of *il1b* and *mmp9* were enhanced in the affected MO2 and MO3 morphants similar to those observed for MO1 (Fig. 3M–R). Because MOs may cause p53-dependent side effects (48), we tested the two MOs that showed highest penetrance of the larval phenotype (MO1 and MO3) in embryos of a p53 mutant (34). Morphological defects and penetrance of the morphant phenotypes were similar in the p53 mutant background as in the wild-type background, demonstrating that the *ptpn6* morphant phenotypes are independent of p53 activation (Supplemental Fig. 1J–L). Because enhanced *mmp9* expression was a major effect in *ptpn6* morphants, we tested the effect of Mmp inhibitors. A combination of two Mmp inhibitors (MMP-2/MMP-9 inhibitor V and a general Mmp inhibitor GM6001) caused a significant shift toward less severe phenotypic defects (Fig. 3S). Thus, we concluded that Mmp inhibitors could dampen the inflammation-associated phenotype in *ptpn6* morphants.

The ptpn6 *morphant phenotype is independent of the presence of microbes*

Because inflammation might be triggered by the presence of microbes, we investigated whether the zebrafish *ptpn6* morphant phenotype also developed in a germ-free environment. To this end, eggs were bleached, treated with iodine, and cultured in the presence of antibiotic and antifungal compounds following established protocols (42). At the end of the experiment, sterility was confirmed by plating culture medium on tryptic soy agar plates, showing that bacterial colonies developed from conventionally reared larvae but not from germ-free cultured larvae. When reared in the germ-free environment, 80–90% of the *ptpn6* morphant larvae developed edema and skin lesions, similar to the conventionally raised morphant larvae. Therefore, the inflammation-associated phenotype of *ptpn6* morphants is apparently not driven by the presence of culturable microbes.

Glucocorticoid treatment enhances the ptpn6 *morphant phenotype*

The immunosuppressive action of glucocorticoids is known to be conserved between zebrafish and mammals (49). Because the *ptpn6* morphant phenotype was associated with enhanced proinflammatory gene expression and leukocyte infiltration of affected tissues, we tested whether these effects could be suppressed by glucocorticoid treatment. Surprisingly, treatment with the synthetic glucocorticoid betamethasone 17-valerate enhanced rather than suppressed the development of edema and skin lesions in *ptpn6* morphants. Betamethasone 17-valerate was previously demonstrated to act as a potent glucocorticoid in zebrafish (50). It significantly reduces wound infiltration by neutrophils in zebrafish larvae (data not shown), confirming its immunosuppressive effect in wild-type fish. The affected tissues in morphants treated with betamethasone 17-valerate were accompanied by a more abundant leukocyte infiltration, as demonstrated using a transgenic marker line for neutrophils (*Tg(mpx:GFP)i114* (35) and by L-plastin immunostaining of neutrophils and macrophages (Fig. 4A–F). In addition, ~10% of *ptpn6* morphants that were treated with betamethasone 17-valerate from 1 dpf died at 5 dpf, whereas all untreated morphants were viable until 7 to 8 dpf. In line with the enhanced phenotype, the induction levels of *il1b* and *mmp9* were also further increased in morphants treated with betamethasone 17-valerate as compared with the control group (Fig. 4G, 4I). The increase of *il1b* and *mmp9* at 5 dpf was more pronounced when betamethasone 17-valerate treatment was performed for 4 d starting at 1 dpf compared with a 2-d treatment starting at 3 dpf (Fig. 4G, 4I). Treatment with two other glucocorticoids, beclomethasone and prednisolone, also enhanced the development of edema and skin lesions (data not shown) and increased *il1b* and *mmp9* expression (Fig. 4H, 4J). However, no general insensitivity to glucocorticoids was observed. Expression of *fkbp5*, a well-known glucocorticoid receptor target gene (49), was inducible by betamethasone 17-valerate in both *ptpn6* morphants and control embryos (data not shown). In addition, betamethasone 17-valerate could still repress the expression of the *pomc* gene in the anterior lobe of the pituitary gland of *ptpn6* morphants (Fig. 4K), a phenotype often used to score for glucocorticoid responsiveness (50). Overall, these results show that glucocorticoids are not able to suppress the inflammatory response observed in *ptpn6* morphants and that instead they unexpectedly enhance this response.

Knockdown of ptpn6 *impairs the ability of embryos to combat* S. typhimurium *and* M. marinum *infections*

To investigate the function of *ptpn6* in the innate immune response to infection, we challenged *ptpn6* morphants and control embryos by i.v. injection of *S. typhimurium* bacteria. Importantly, bacterial injections were performed at 28 hpf (i.e., several days before the appearance of inflammation and other phenotypic effects in *ptpn6* morphants). In both *ptpn6* morphants and controls, *S. typhimurium* infection was lethal ~24–30 hpi. However, CFU counts at 2, 8, and 20 hpi showed that *S. typhimurium* accumulated faster in the *ptpn6* morphants (Fig. 5A). Subsequently, we performed infections with the nonpathogenic *S. typhimurium* LPS *O*-Ag mutant strain Ra (44). Although this Ra strain hardly accumulated in control embryos, clear accumulation of the DsRed-labeled Ra bacteria was observed in ~55% of *ptpn6* MO1 morphants at 1 d postinfection (dpi) (Fig. 5B–D). At 5 dpi, control embryos had cleared the infection or showed very low DsRed fluorescence signal, whereas the majority of *ptpn6* morphants were heavily infected or had died at 5 dpi (Fig. 5B, 5E, 5F). Increased accumulation of *S. typhimurium* Ra bacteria was also observed in

mean ± SEM of three independent experiments. Asterisks indicate significant differences tested by two-way ANOVA analysis with Bonferroni method as post hoc test. BV treatment did not significantly affect *il1b* and *mmp9* expression in the control groups. Data in (H) and (J) represent two individual experiments with 2 or 4 d of glucocorticoid treatment. (**K**) Glucocorticoid repression of *pomc* expression in the anterior lobe of the pituitary gland in *ptpn6* morphants and control embryos. Double-transgenic zebrafish embryos expressing prolactin:rfp in the anterior lobe of the pituitary gland and pomc:gfp in the anterior and posterior lobes [*Tg(-1.0pomca:GFP)zf44;Tg(prl:RFP)zf113*] (37) were injected with standard control (con) or *ptpn6* (MO1) MOs and treated from 1 dpf with 1 μM BV in 0.1% DMSO or with vehicle (0.1% DMSO) as a control. The pituitary gland was imaged at 5 dpf, and confocal Z-stacks are representative of 15–20 embryos per group. In *ptpn6* morphants, the pituitary gland is twisted to the right compared with that in control embryos, but pomc:gfp expression in the anterior lobe is downregulated by glucocorticoid treatment, similar to the control embryos. Scale bars, 20 μm. $*p < 0.05$, $**p < 0.01$, $***p < 0.001$.

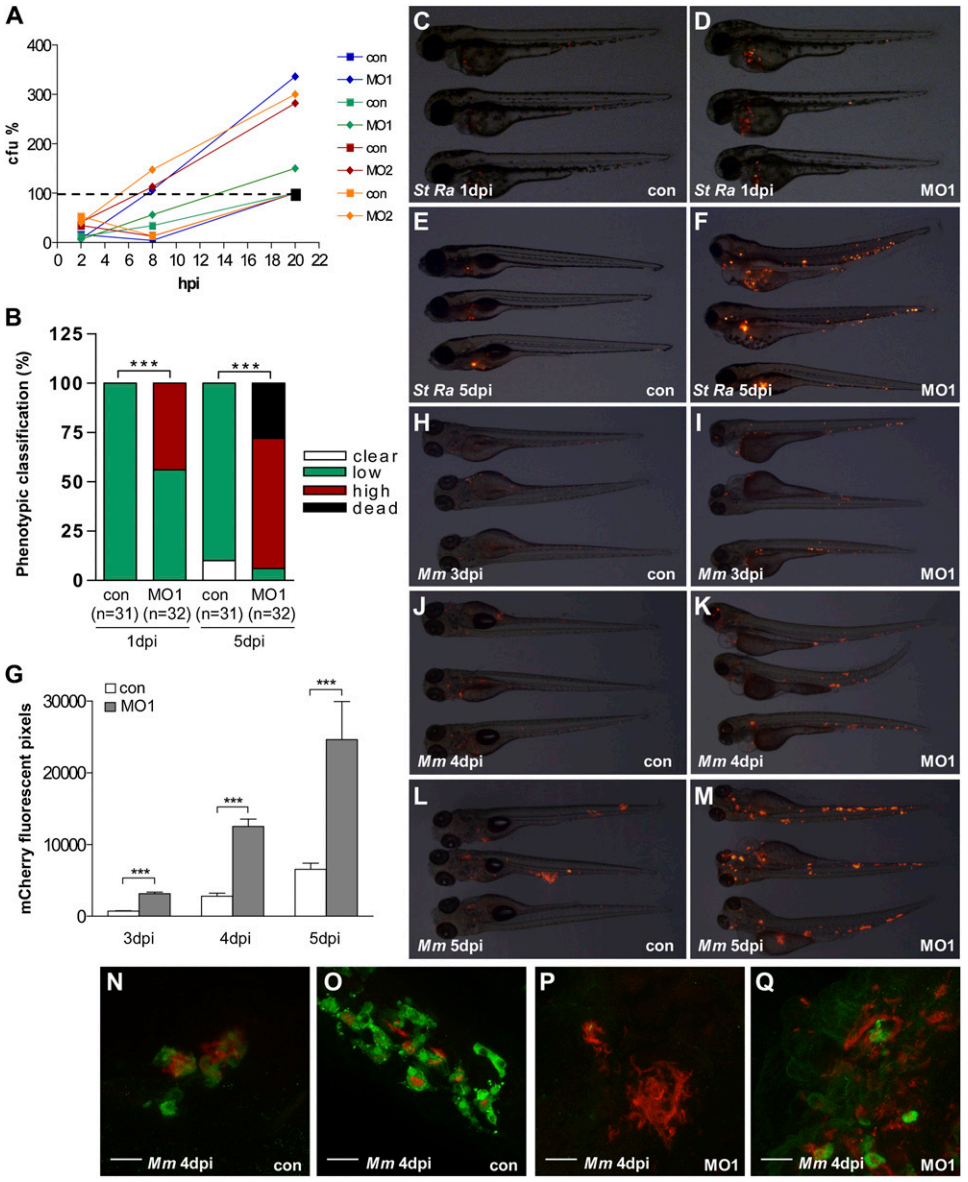

FIGURE 5. Impaired control of *S. typhimurium* and *M. marinum* infection in *ptpn6* morphants. (**A**) Infection with *S. typhimurium* wild-type strain. Embryos were injected with standard control MO (con) or *ptpn6* (MO1, MO2) MOs and infected with *S. typhimurium* at 28 hpf. Groups of five embryos were crushed in PBS at 2, 8, and 20 hpi, and dilutions were plated for CFU counting on Luria-Bertani medium with carbenicillin selection of the DsRED marker plasmid in *S. typhimurium*. Four independent experiments (two with each MO) are shown. Control and MO groups that belong to one experiment are indicated with the same colors. In each experiment, the CFU count data are expressed relative to the CFU value of the control group at the end point of analysis (20 hpi), which was set at 100% (dashed line indicates the 100% level). In all four experiments, the relative CFU values of the morphant group at 8 and 20 hpi were above those of the control group at the same time points. (**B**–**F**) Infection with *S. typhimurium* LPS *O*-Ag mutant Ra strain (*St Ra*). Embryos were injected with standard control (con) or *ptpn6* (MO1) MOs and infected with *S. typhimurium* Ra at 28 hpf. The bacterial burden was analyzed at 1 and 5 dpi based on fluorescence of the DsRED marker plasmid. A quantification of phenotypes (B) and stereo fluorescence images (lateral view, anterior to the *left*) of three embryos per group (C–F) are shown for a representative example of three independent experiments. The bacterial burden in embryos at 1 dpi was scored as low (representative image in C) or high (representative image in D). At 5 dpi, embryos had cleared the infection, had died, or showed low (representative image in E) or high (representative image in F) bacterial burden. Differences between con and MO1 groups in (B) were significant by a χ^2 test. (**G**–**Q**) Infection with *M. marinum* Mma20 strain (*Mm*). Embryos were infected with ~100 CFU at 28 hpf, and formation of *M. marinum* granulomas was analyzed at 3, 4, and 5 dpi based on fluorescence of the mCherry marker plasmid. Fluorescence images of >60 embryos per treatment group accumulated from two independent experiments were analyzed with pixel quantification software (47) including an uninfected group as the blank. Pixel quantification data ± SEM (G) and representative fluorescence images (lateral view, anterior to the *left*) of three embryos per group (H–M) are shown. Differences between con and MO1 groups were significant by unpaired *t* test. (N–Q) Confocal Z-stacks of granulomas in *ptpn6* MO1 morphants and control embryos with L-plastin immunofluorescence in green and *M. marinum* fluorescence in red. Scale bars, 20 μm. ***$p < 0.001$.

embryos injected with *ptpn6* MO2 or MO3 (Supplemental Fig. 1M–Q).

Next, we examined the response of *ptpn6* morphants to infection with *M. marinum*, a pathogen known to cause a chronic infection in zebrafish embryos, whereby infected and uninfected macrophages cluster into aggregates that resemble tuberculous granulomas (51, 52). At 3 dpi, *ptpn6* morphants showed increased fluorescence signal of mCherry-labeled *M. marinum* bacteria and increased numbers of granuloma-like aggregates compared with control embryos (Fig. 5G–I, Supplemental Fig. 1R, 1S). At 4 and

5 dpi, granulomas in *ptpn6* morphants further increased in size compared with those in control embryos (Fig. 5G, 5J–M). Furthermore, immunohistochemical analysis of granulomas at 4 dpi showed that the bacteria were mostly extracellular in *ptpn6* morphants, whereas in control embryos, bacteria were mostly contained within L-plastin–labeled leukocytes (Fig. 5N–Q).

In conclusion, when challenged with bacteria during early development, prior to the manifestation of the late inflammation-associated phenotype, *ptpn6* morphants were severely impaired in their ability to control the progression of infection. This impaired control was observed with *S. typhimurium* and *M. marinum* strains that induce very different pathologies, indicating a general inability of *ptpn6* morphants to mount a functional immune response.

Bacterial challenge of ptpn6 *morphants leads to hyperinduction of* il1b *and* mmp9 *gene expression*

To further investigate the function of *ptpn6* in the innate immune response to infection, we performed qPCR analysis for two genes, *il1b* and *mmp9*, which were previously shown to represent robust proinflammatory markers associated with bacterial infection (38) and with the late phenotype observed after *ptpn6* knockdown (see above). We chose to analyze the response to *S. typhimurium* infection at 8 hpi (36 hpf) based on a previous time-course analysis (38). As expected, control embryos showed a strong induction of *il1b* and *mmp9* expression levels. Upon knockdown of *ptpn6* with the different MOs, the induction levels of *il1b* and *mmp9* were significantly higher than in the control embryos (Fig. 6A–D). Increased induction of these genes was also observed in p53 mutant background (data not shown). These data suggest that *ptpn6* functions as a negative regulator of *il1b* and *mmp9* induction during *S. typhimurium* infection. Unlike the strong proinflammatory gene expression that is induced by *S. typhimurium* infection at 8 hpi (Fig. 6A–D), control embryos or *ptpn6* morphants infected with *M. marinum* did not show significant *il1b* and *mmp9* induction at this time point (Fig. 6E, 6F). However, at 3 dpi, *mmp9* (but not *il1b*) expression was increased in *M. marinum*–infected *ptpn6* morphants compared with uninfected morphants and infected controls (Fig. 6E, 6F). In summary, a hyperinduction of proinflammatory genes was observed upon bacterial infections of *ptpn6* morphants, yet their ability to control these infections was impaired.

Microarray analysis demonstrates an overall enhancement of the innate immune response to S. typhimurium *infection upon* ptpn6 *knockdown*

The *S. typhimurium* infection model was chosen for further investigation of the specific effects of *ptpn6* knockdown on the innate immune response by microarray analysis. The advantage of this model for functional analysis of *ptpn6* was that the response to *S. typhimurium* infection can be analyzed at 36 hpf (8 hpi) (38, 53), thus avoiding that the microarray analysis is affected by secondary effects of the late inflammatory phenotype (observed at 4–6 dpf). RNA samples from infected and mock-injected *ptpn6* MO1 morphants or control embryos from three replicate experiments were analyzed using a common reference approach (Fig. 7). First, we analyzed the basal expression differences between mock-injected *ptpn6* morphants and control embryos. KEGG pathway analysis showed that p53 signaling and cell cycle were the most significantly affected pathways, and minor effects were observed on cytosolic DNA sensing, sucrose metabolism, and pyrimidine metabolism (Fig. 7B). There was little overlap with the genes that were induced by infection in *ptpn6* morphants: only 7% of the microarray probes that showed basal expression differences between controls and *ptpn6* morphants were responsive to infection in *ptpn6* morphants (Fig. 7B). The infection-responsive gene set showed significant alteration of many KEGG pathways related to the immune response, such as TLR, NLR, RIG-I, p53, MAPK, and JAK–STAT signaling (Fig. 7B). For further analysis of *ptpn6* function, we concentrated on the differences between the responses to infection in *ptpn6* morphants and controls.

The total number of probes showing significant responsiveness to infection was ~2-fold larger in *ptpn6* morphants than in controls (Fig. 7C). Furthermore, the absolute fold changes of many

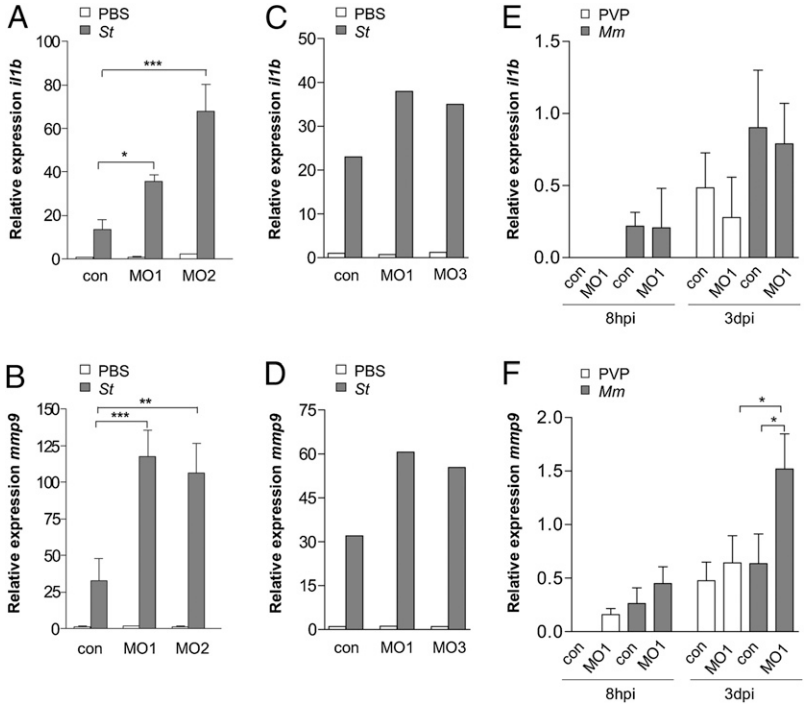

FIGURE 6. Increased induction of *il1b* and *mmp9* expression in *ptpn6* morphants challenged with bacterial pathogens. Effect of *ptpn6* knockdown on *il1b* (**A**, **C**) and *mmp9* (**B**, **D**) expression in response to *S. typhimurium* infection. Embryos were injected at the 1 to 2 cell stage with standard control (con) or *ptpn6* (MO1, MO2, MO3) MOs and injected with 250 CFU of *S. typhimurium* (*St*) or mock-injected with PBS at 28 hpf. RNA was isolated for qPCR analysis at 8 hpi. Relative expression levels are shown with the uninfected control group set at 1. Data for MO1 and MO2 (A, B) are the mean ± SEM of three replicate experiments, and the phenocopy with MO3 (C, D) is shown in an additional independent experiment. Asterisks indicate significant differences tested by two-way ANOVA analysis with Bonferroni method as post hoc test. Effect of *ptpn6* knockdown on *il1b* (**E**) and *mmp9* (**F**) expression in response to *M. marinum* infection. Embryos were injected at the 1 to 2 cell stage with standard control (con) or *ptpn6* MO (MO1) and injected with 100 CFU of *M. marinum* (*Mm*) or mock-injected with polyvinylpyrrolidone (PVP) carrier solution at 28 hpf. RNA was isolated for qPCR analysis at 8 hpi and 3 dpi. Data are plotted on a logarithmic scale and are the mean ± SEM of three replicate experiments. Asterisks indicate significant differences tested by two-way ANOVA analysis with Bonferroni method as post hoc test. $*p < 0.05$, $**p < 0.01$, $***p < 0.001$.

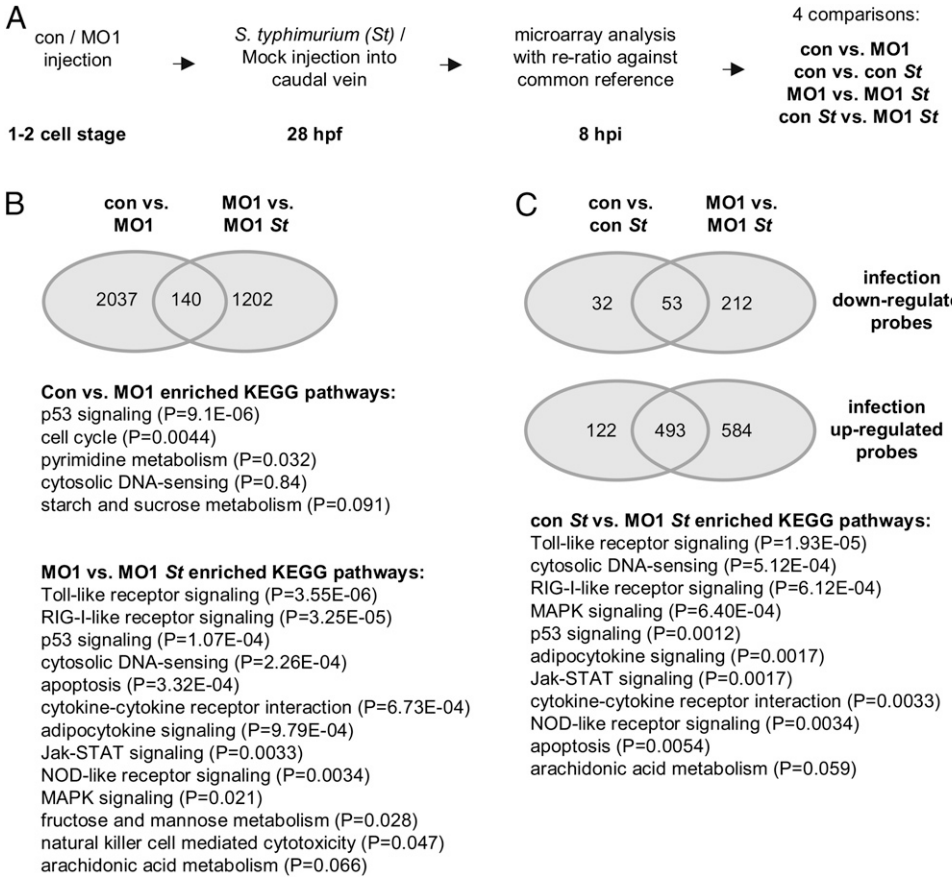

FIGURE 7. Enhanced innate immune response to *S. typhimurium* in *ptpn6* morphants. (**A**) Experimental setup of the microarray analysis. Embryos were injected with *ptpn6* MO (MO1) or Danieau's buffer (con) at the 1 to 2 cell stage, and ~250 CFU of *S. typhimurium* (*St*) bacteria were injected into the caudal vein at 28 hpf after the onset of the blood circulation, or PBS was injected as a control. Microarray analysis was performed on RNA samples extracted from pools of 15–20 embryos at 8 hpi. RNA samples from the four treatment groups (con/PBS, con/*St*, MO1/PBS, and MO1/*St*) were obtained from three independent experiments and hybridized against a common reference consisting of RNA from all treatment groups. Next, four expression ratios were derived by Rosetta Resolver reratio analysis of the sample data against the common reference. The significance cutoffs were set at an absolute fold change ≥ 1.5 and $p \leq 0.0001$. (**B**) Venn diagram showing the overlap between the effect of *ptpn6* knockdown on basal gene expression levels (con versus MO1) and the effect of *S. typhimurium* on gene expression in *ptpn6* morphants (MO1 versus MO1 *St*). The numbers of probes with significantly changed expression are shown in the Venn diagram, and significantly enriched KEGG pathways for each comparison are indicated below. (**C**) Venn diagrams showing comparisons of the numbers of probes that were up- or downregulated by *S. typhimurium* infection in control embryos (con versus con *St*) or in *ptpn6* morphants (MO1 versus MO1 *St*). KEGG pathways that were significantly enriched in the dataset of infected *ptpn6* morphants compared with the dataset of infected controls (con *St* versus MO1 *St*) are indicated below. A complete overview of the microarray data is given in Supplemental Table I.

infection-responsive probes were larger in *ptpn6* morphants (see Supplemental Table I for a complete overview of the microarray data). In fact, a total of 598 probes (representing 258 different genes) showed significantly higher upregulation in *ptpn6* morphants, and 78 probes (representing 51 different genes) showed significantly stronger downregulation (Fig. 8). Analysis of the gene group with higher upregulation in *ptpn6* morphants showed significant overrepresentation of TLR, NLR, RIG-I, p53, MAPK, JAK–STAT, and other immune-related KEGG pathways (Fig. 7C). More specifically, genes showing higher upregulation in *ptpn6* morphants included cytokine/chemokine/IFN genes such as *il1b*, *il8*, *tnfa*, *tnfb*, and *ifnphi1*, Mmps such as *mmp9* and *mmp13*, and many transcriptional regulators of the ATF, CEBP, AP-1, NF-κB, and STAT families (Fig. 8). The higher upregulation of *il1b* and *mmp9* was consistent with the qPCR experiments described above (Fig. 6A, 6B) and with qPCR validation of the samples used for the microarray study (Supplemental Fig. 2A, 2B). As observed in previous *S. typhimurium* infection studies, several negative regulators of immunity signaling are induced concomitantly with the induction of proinflammatory genes (38, 53). Similar to the increased induction of proinflammatory genes, infected *ptpn6* morphants also showed increased induction levels of several of these negative regulators, such as *irak3*, *socs3a*, and *socs3b*, and NF-κB inhibitor genes (*nfkbiaa*, *nfkbiab*, *nfkbib*, and *nfkbiz*). In contrast, the anti-inflammatory cytokine gene *il10* (represented by four probes on the array) did not show increased induction in *ptpn6* morphants.

The smaller gene group that showed stronger downregulation upon infection in *ptpn6* morphants than in the controls included two CCL chemokine genes (*ccl1* and *ccl–c11a*) and several leukocyte markers such as *coro1a*, *cpa5*, *cxcr3.2*, *lgals9l1*, *lcp1*, *lyz*, and *mpx* (Fig. 8). However, there was no generally enhanced downregulation of leukocyte markers in infected *ptpn6* morphants, as *mpeg1* was less repressed in infected *ptpn6* morphants than in infected controls, and *csf1r* and *mfap4* showed unaltered expression under all conditions. qPCR analysis of leukocyte markers showed the same trend as the microarray data, particularly increased downregulation of *lgals9l1*, *lyz*, and *mpx* during infection, less pronounced downregulation of *mpeg1,* and unaltered expression of other markers, including *csf1r* and *mfap4* (Supplemental Fig. 2C–F).

In conclusion, microarray analysis indicated that under *ptpn6* knockdown conditions, embryos responded to *S. typhimurium*

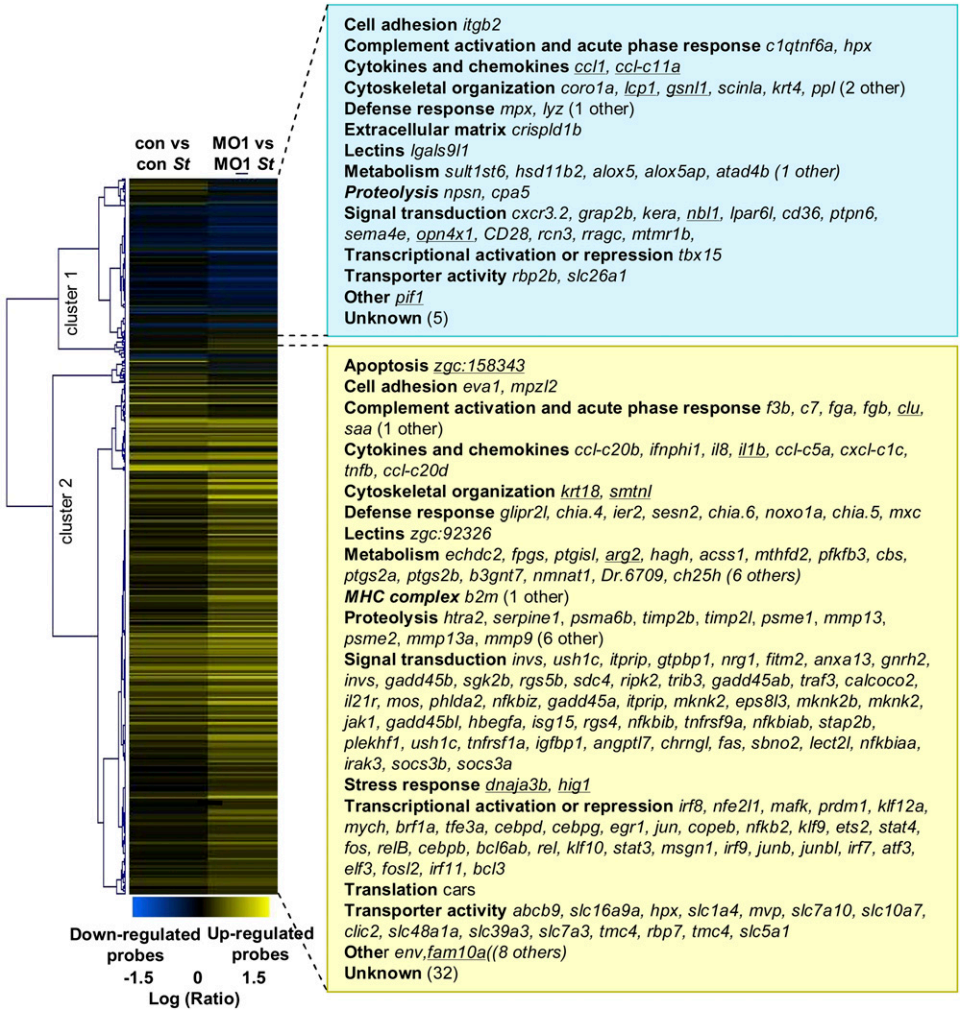

FIGURE 8. Gene groups showing higher upregulation or stronger downregulation upon *S. typhimurium* challenge of *ptpn6* morphants compared with *S. typhimurium* challenge of control embryos. A two-dimensional hierarchical clustering (average link, cosine correlation) was performed of the probes that were upregulated or downregulated by *S. typhimurium* (*St*) infection in control embryos (con) or in *ptpn6* morphants (MO1) (fold change $\geq$1.5; $p \leq 0.0001$). Upregulated probes are indicated by increasingly brighter shades of yellow, and downregulated probes are indicated by increasingly brighter shades of blue. Cluster 1 contains 78 probes (representing 51 different genes) that showed a stronger downregulation in *S. typhimurium*–infected *ptpn6* morphants than *S. typhimurium*–infected control embryos, and cluster 2 contains 598 probes (representing 258 different genes) with stronger upregulation in the *ptpn6* morphants. The gene symbols corresponding to the probes with stronger up- or downregulation are indicated next to the two clusters, categorized in functional annotation groups. Only gene symbols of genes with assigned gene names are indicated in the figure, and the number of other genes without a gene name in each annotation group is indicated in parentheses; the full list is given in Supplemental Table I. Symbols of genes that also showed differential expression in mock-injected *ptpn6* morphants compared with mock-injected control embryos are underlined.

infection by an enhanced gene induction profile of the innate immune response.

Increased proinflammatory gene induction in S. typhimurium–*infected* ptpn6 *morphants is confirmed by RT-MLPA analysis*

In addition to the microarray analysis, we used a recently described RT-MLPA assay that allows the simultaneous semiquantitative PCR analysis of 34 innate immune genes (41). Further confirming the microarray results, RT-MLPA analysis showed >2-fold increased *S. typhimurium*–induced upregulation in *ptpn6* morphants compared with controls for several cytokine/chemokine/IFN genes (*ccl-c5a*, *cxcl-c1c*, *ifnphi1*, *il1b*, *il8*, and *tnfa*), immune-related transcription factor genes (*fos*, *jun*, *junb*, *nfkb2*, and *rel*), the Mmp gene *mmp9*, and the acidic chitinase gene *chia.6* (Fig. 9). Additionally, five other genes that did not meet the significance thresholds in the microarray analysis (*ccl20*, *ccl-c24i*, *cxc46*, *fkbp5*, and *tlr5a*) also showed >2-fold higher upregulation in *ptpn6* morphants based on RT-MLPA (Fig. 9). Of note, in both microarray and RT-MLPA analysis, the anti-inflammatory *il10* gene showed equal induction levels during *S. typhimurium* infection of *ptpn6* morphants and controls (Fig. 9, Supplemental Table I). The increased proinflammatory gene induction profile of *S. typhimurium*–infected *ptpn6* morphants, observed in microarray analysis and RT-MLPA, is consistent with a function of *ptpn6* as a negative regulator of the innate immune response upon infection (Fig. 10).

Discussion

The association of SHP1/PTPN6 deficiency with several types of chronic inflammatory disorders and with lymphoid and myeloid malignancies has raised substantial interest in this hematopoietic phosphatase as a drug target (54). In this study, we exploited the zebrafish embryo as a novel animal model for studies on the function of the *ptpn6* gene. The late onset of adaptive immunity during zebrafish development permits studying *ptpn6* function in the sole context of innate immunity during embryo and larval

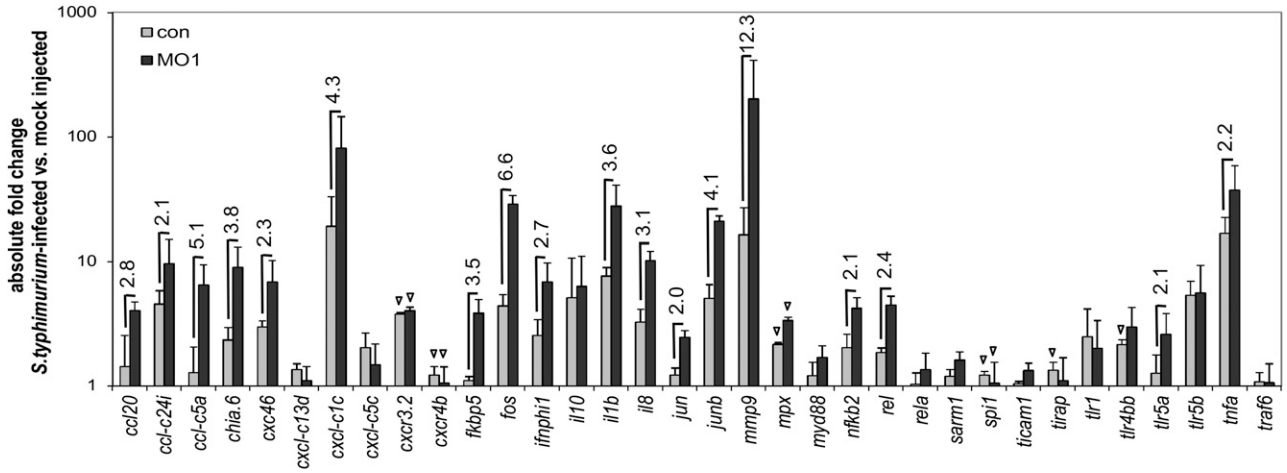

FIGURE 9. Hyperinduction of proinflammatory genes in *S. typhimurium*–infected *ptpn6* morphants shown by RT-MLPA analysis. Relative expression levels of 34 innate immune response genes were determined as described in Rotman et al. (41). The figure shows the absolute fold difference in expression of *S. typhimurium*–infected control embryos (con) and *ptpn6* morphants (MO1) versus the corresponding mock-injected groups. Data are plotted on a logarithmic scale. Values are the means ± SD of three independent sample sets, which were the same as previously used for microarray analysis. Downregulated expression is indicated with triangles. Numbers indicate ≥2-fold-change differences in upregulated expression between *S. typhimurium*–infected *ptpn6* morphants and *S. typhimurium*–infected control embryos.

development. Our results show that *ptpn6* deficiency in this model leads to pleiotropic defects at the late larval stage, accompanied by leukocyte infiltration and upregulated inflammatory gene expression. Moreover, when embryos were challenged with bacteria during earlier stages of development, *ptpn6* knockdown enhanced the innate immune response to this infection. Despite this increased inflammatory response, *ptpn6*-deficient embryos were severely impaired in their ability to control infections, supporting the crucial importance of negative regulation by *ptpn6* for a balanced and functional innate immune response.

Inflammation-associated effects of ptpn6 deficiency

Under normal culture conditions, without challenge by infection, *ptpn6* morphant larvae developed severe edema and skin lesions by 5 to 6 d of age. The affected tissues in zebrafish *ptpn6* morphants were strongly infiltrated by leukocytes, and increased numbers of TUNEL-positive apoptotic cells were also detected in these areas. Simultaneously, the overall expression levels of proinflammatory markers *il1b* and *mmp9* were >10-fold increased. Because *ptpn6* mRNA injection induced ectopic overexpression artifacts, we have not been able to confirm the specificity of the phenotype by mRNA rescue. However, several other lines of evidence support the specificity of the phenotype. First, similar phenotypes were observed with three different MOs against *ptpn6*. Second, MO injection in p53 mutant background showed that the phenotype was not due to p53 activation, which is a common cause of MO side effects (48). Third, treatment with Mmp inhibitors could dampen the severity of the phenotype, supporting the relation between the phenotypic defect and inflammation.

The *ptpn6* knockdown phenotype in zebrafish is highly reminiscent of the severe skin inflammation observed in murine *Ptpn6* mutants *me*, *mev*, and *spin* (11, 12, 16). In mice, *Ptpn6* deficiency, besides causing inflammation, was also associated with hyperproliferation of immune cells (55), but we did not detect enhanced proliferation of myeloid cells during zebrafish embryonic and larval development. Among the three mutant alleles of *Ptpn6* in mice, *spin* causes the least severe functional knockdown (16). Inflammatory foot lesions of *spin* mutants did not develop when homozygotes were raised in a germ-free environment, showing the requirement of the normal microbiota to trigger this phenotype (16). However, *me* homozygotes born into a specific pathogen-free colony survived no better than under conventional conditions (56). Similarly, we found that the late inflammation-associated phenotype of *ptpn6* morphant zebrafish larvae was equally severe when cultured using an established protocol to generate germ-free conditions (42). Complete germ-free conditions cannot be guaranteed during MO injections, but at least a major reduction of microbes was achieved in our experiments, because no bacterial colonies were observed when the culture medium of MO-injected larvae was plated on rich culture medium. Therefore, like in the *me* mutant, most likely another mechanism than the response to microbes is responsible for the development of spontaneous inflammation in *ptpn6* morphants.

In addition to the general inflammation-associated defects in *ptpn6* morphants, the dorsal area of the brain contained increased numbers of apoptotic cells as well as increased numbers of cells positive for the proliferation marker phosphohistone H3. Deregulation of pathways such as MAPK and NF-κB signaling, known to be affected by mammalian SHP1, may explain enhanced proliferation and apoptotic cell numbers in *ptpn6* morphants. The expression of *ptpn6* in wild-type embryos and larvae by WISH was only detectable in myeloid cells and in the larval thymus (31). However, it cannot be excluded that *ptpn6* is also expressed in other tissues at lower levels, which may explain the specific hyperproliferative area in the brain of *ptpn6* morphants. In rodents, *Ptpn6* expression is also predominantly hematopoietic, but has been detected in other tissues as well, including the CNS (57, 58).

Treatment with glucocorticoids enhanced the inflammatory phenotype, which is surprising because glucocorticoids are well known for their anti-inflammatory effects. They are widely used clinically to treat a variety of human immune-related diseases (59) and their immune-suppressive effects appear to be well conserved between mammals and fish (49). Most anti-inflammatory effects of glucocorticoids are a result of the inhibitory interaction between the glucocorticoid receptor (GR) and transcription factors like AP-1 and NF-κB, which are important for the upregulation of many proinflammatory genes (60). However, interaction with other transcription factors can enhance the activity of these proteins, and this may even lead to specific proinflammatory effects of glucocorticoids. In particular, interactions between GR and

members of the STAT family, like STAT3, -5, and -6, have been demonstrated to be synergistic in nature (61–66) Interestingly, the JAK–STAT signaling pathway has been shown to be negatively regulated by SHP1 in many studies (67). Thus, the enhancement of the inflammatory phenotype upon *ptpn6* knockdown in zebrafish by glucocorticoids might be explained by a synergistic interaction between the GR and transcription factors, like the members of the STAT family, that have become activated due to the Ptpn6 deficiency (Fig. 10) . Because in humans SHP1/PTPN6 deficiency has been shown to be possibly involved in the pathogenesis of several immune-related diseases, care should be taken when patients suffering from these diseases are treated with glucocorticoids. The SHP1 deficiency could be the cause of resistance to glucocorticoid treatment that is observed in a significant subpopulation of patients (68) and could theoretically even underlie a worsening of the disease state in response to this therapy.

Function of ptpn6 *in the response to bacterial infections*

Knockdown of *ptpn6* impaired the ability of zebrafish embryos to control infections with two bacterial pathogens that induce very different disease pathologies in the zebrafish embryo model: *S. typhimurium*, which causes acute disease, and *M. marinum*, which causes a chronic disease in which bacteria persist in granulomatous aggregates. Even the growth of a normally nonpathogenic strain (*S. typhimurium* LPS *O*-Ag Ra mutant) could not be efficiently controlled and caused lethality. In contrast, murine *spin* mutants displayed increased resistance to *Listeria monocytogenes* (16). As discussed above, the *spin* phenotype is ascribed to a hypomorphic allele of *Ptpn6*, which may explain why this mutant is immunocompetent, whereas zebrafish *ptpn6* morphants are not. The immunodeficiency of *ptpn6* morphants was apparent at early developmental stages well before the spontaneous increase in basal levels of proinflammatory genes and developmental defects that occur later during larval development. We found that the expression levels of immune-related transcription factor genes and many effector genes of the innate immune response were hyperinduced upon infection in *ptpn6* morphants. In agreement, the whole set of hyperinduced genes showed significant enrichment of KEGG pathways related to pathogen recognition and cytokine signaling. These results support the function of *ptpn6* as a negative regulator of the innate immune response to bacterial infection. We observed hyperinduction of innate immune response genes with three different *ptpn6* MOs, whereas we have found that the induction of these genes is reduced by several MOs targeting other immune genes, including *myd88* and *traf6* (38, 69). Because *ptpn6* morphants displayed decreased resistance, the hyperactivation of their innate immune response is apparently contraproductive for the organism's defense against bacterial pathogens.

The hyperinduction of innate immune response genes upon infection of *ptpn6* morphants was specific, because, for example, the expression levels of several myeloid markers were unchanged or reduced. In addition to many proinflammatory cytokines and transcription activators of the immune response, we also observed hyperinduction of other negative regulators than *ptpn6* itself. Apparently, in the absence of *ptpn6*, increased induction of other negative regulators was insufficient to prevent excessive inflammation and a contraproductive defense response against bacterial pathogens. This may be explained by the presumed inhibitory effect of Ptpn6 on many cytokine and immunoreceptors as well as central kinases in innate immunity signaling pathways (9, 10) (Fig. 10). Furthermore, the anti-inflammatory cytokine gene *il10* was not induced to higher levels in infected *ptpn6* morphants than in controls. The fact that increased production of proinflammatory cytokines is not counteracted in *ptpn6* morphants by increased anti-inflammatory IL-10 production is a possible explanation for their nonfunctional immune response against bacterial pathogens.

Interestingly, virulence factors of *Leishmania* parasites have been proposed to block macrophage functions by activation of SHP1 (9, 70). Similarly, SHP1 activation by lipoarabinomannan has been suggested as a host-evasion strategy of *Mycobacterium tuberculosis* (71, 72). Our results show the important regulatory function of this phosphatase in the host innate immune response to bacterial pathogens, which therefore could indeed be an attractive target for bacteria to manipulate. In our study, deficiency of *ptpn6* favored growth of *S. typhimurium* and *M. marinum* despite an enhanced innate immune response to these pathogens. These results are in line with studies of zebrafish embryos defective in TNF signaling or eicosanoid biosynthesis, which indicated that the outcome of *M. marinum* infection is worsened either when the fish produce high levels of anti-inflammatory lipoxins inhibiting TNF production or when the fish produce proinflammatory leukotrienes and excessive levels of TNF (73–75). We propose that the role of

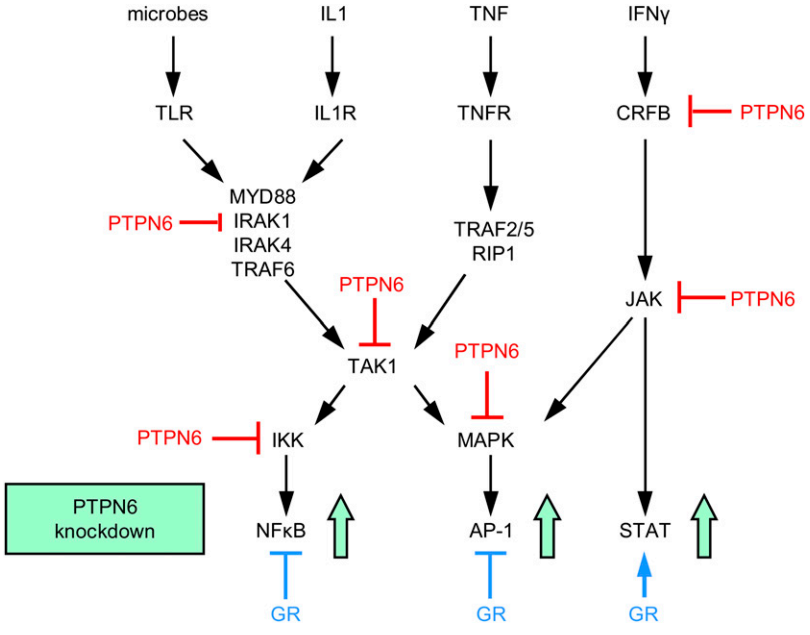

FIGURE 10. Model of PTPN6/SHP1 function in innate immunity signaling and interaction with glucocorticoid signaling. PTPN6/SHP1 has been proposed to inhibit cytokine receptors (like the CRFB family) as well as several kinases in TLR and cytokine signaling pathways (9, 10). The putative inhibition motifs in these proteins are evolutionary conserved (Supplemental Table II). Under conditions of PTPN6 deficiency, the activation of transcriptional regulators like NF-κB, AP-1, and STATs is enhanced (green arrows). Upon stimulation with glucocorticoids, the GR inhibits NF-κB and AP-1 activity, but may have a synergistic interaction with STATs.

ptpn6 is crucial for tightly regulating the induction levels of many key players in the innate immune response, identified by our microarray analysis, and conclude that the loss of *ptpn6* function results in a nonfunctional immune response to *S. typhimurium* and *M. marinum* infections.

Acknowledgments

We thank Mark van Eekelen and Vincent Runtuwene for initial experiments with the *ptpn6* splice morpholino MO1, Janneke Rotman (BaseClear B.V., Leiden, The Netherlands) for help with RT-MLPA analysis, Gerda Lamers for assistance with microscopy, Ulrike Nehrdich and Davy de Witt for fish care, and Peter Schoonheim and other group members for sharing protocols and helpful discussions. We also thank Steven Renshaw (University of Sheffield, Sheffield, U.K.) for the mpx:gfp line, Brant Weinstein (National Institute of Child Health and Human Development, Bethesda, MD) for the fli1:EGFP line, Shlomo Melmed (Cedars-Sinai Medical Center, Los Angeles, CA) for the *pomc:gfp/prl:rfp* line, Anna Huttenlocher (University of Wisconsin, Madison, WI) for L-plastin Ab, and Astrid van der Sar (VU Medical Center, Amsterdam, The Netherlands) for bacterial strains and plasmids.

Disclosures

The authors have no financial conflicts of interest.

References

1. Beutler, B. 2009. Microbe sensing, positive feedback loops, and the pathogenesis of inflammatory diseases. *Immunol. Rev.* 227: 248–263.
2. Drexler, S. K., and B. M. Foxwell. 2010. The role of toll-like receptors in chronic inflammation. *Int. J. Biochem. Cell Biol.* 42: 506–518.
3. Theofilopoulos, A. N., D. H. Kono, B. Beutler, and R. Baccala. 2011. Intracellular nucleic acid sensors and autoimmunity. *J. Interferon Cytokine Res.* 31: 867–886.
4. O'Neill, L. A. 2008. When signaling pathways collide: positive and negative regulation of toll-like receptor signal transduction. *Immunity* 29: 12–20.
5. Zhang, J., A. K. Somani, and K. A. Siminovitch. 2000. Roles of the SHP-1 tyrosine phosphatase in the negative regulation of cell signalling. *Semin. Immunol.* 12: 361–378.
6. Tsui, F. W., A. Martin, J. Wang, and H. W. Tsui. 2006. Investigations into the regulation and function of the SH2 domain-containing protein-tyrosine phosphatase, SHP-1. *Immunol. Res.* 35: 127–136.
7. Pao, L. I., K. Badour, K. A. Siminovitch, and B. G. Neel. 2007. Nonreceptor protein-tyrosine phosphatases in immune cell signaling. *Annu. Rev. Immunol.* 25: 473–523.
8. Yi, T. L., J. L. Cleveland, and J. N. Ihle. 1992. Protein tyrosine phosphatase containing SH2 domains: characterization, preferential expression in hematopoietic cells, and localization to human chromosome 12p12-p13. *Mol. Cell. Biol.* 12: 836–846.
9. Abu-Dayyeh, I., M. T. Shio, S. Sato, S. Akira, B. Cousineau, and M. Olivier. 2008. *Leishmania*-induced IRAK-1 inactivation is mediated by SHP-1 interacting with an evolutionarily conserved KTIM motif. *PLoS Negl. Trop. Dis.* 2: e305.
10. Abu-Dayyeh, I., B. Ralph, L. Grayfer, M. Belosevic, B. Cousineau, and M. Olivier. 2010. Identification of key cytosolic kinases containing evolutionarily conserved kinase tyrosine-based inhibitory motifs (KTIMs). *Dev. Comp. Immunol.* 34: 481–484.
11. Shultz, L. D., P. A. Schweitzer, T. V. Rajan, T. Yi, J. N. Ihle, R. J. Matthews, M. L. Thomas, and D. R. Beier. 1993. Mutations at the murine motheaten locus are within the hematopoietic cell protein-tyrosine phosphatase (Hcph) gene. *Cell* 73: 1445–1454.
12. Tsui, H. W., K. A. Siminovitch, L. de Souza, and F. W. Tsui. 1993. Motheaten and viable motheaten mice have mutations in the haematopoietic cell phosphatase gene. *Nat. Genet.* 4: 124–129.
13. Kozlowski, M., I. Mlinaric-Rascan, G. S. Feng, R. Shen, T. Pawson, and K. A. Siminovitch. 1993. Expression and catalytic activity of the tyrosine phosphatase PTP1C is severely impaired in motheaten and viable motheaten mice. *J. Exp. Med.* 178: 2157–2163.
14. Yu, C. C., H. W. Tsui, B. Y. Ngan, M. J. Shulman, G. E. Wu, and F. W. Tsui. 1996. B and T cells are not required for the viable motheaten phenotype. *J. Exp. Med.* 183: 371–380.
15. Zhang, L., S. Y. Oh, X. Wu, M. H. Oh, F. Wu, J. T. Schroeder, C. M. Takemoto, T. Zheng, and Z. Zhu. 2010. SHP-1 deficient mast cells are hyperresponsive to stimulation and critical in initiating allergic inflammation in the lung. *J. Immunol.* 184: 1180–1190.
16. Croker, B. A., B. R. Lawson, S. Rutschmann, M. Berger, C. Eidenschenk, A. L. Blasius, E. M. Moresco, S. Sovath, L. Cengia, L. D. Shultz, et al. 2008. Inflammation and autoimmunity caused by a SHP1 mutation depend on IL-1, MyD88, and a microbial trigger. [Published erratum appears in 2008 *Proc. Natl. Acad. Sci. USA* 105: 19561.] *Proc. Natl. Acad. Sci. USA* 105: 15028–15033.
17. Croker, B. A., R. S. Lewis, J. J. Babon, J. D. Mintern, D. E. Jenne, D. Metcalf, J. G. Zhang, L. H. Cengia, J. A. O'Donnell, and A. W. Roberts. 2011. Neutrophils require SHP1 to regulate IL-1β production and prevent inflammatory skin disease. *J. Immunol.* 186: 1131–1139.
18. An, H., J. Hou, J. Zhou, W. Zhao, H. Xu, Y. Zheng, Y. Yu, S. Liu, and X. Cao. 2008. Phosphatase SHP-1 promotes TLR- and RIG-I-activated production of type I interferon by inhibiting the kinase IRAK1. *Nat. Immunol.* 9: 542–550.
19. Eriksen, K. W., A. Woetmann, L. Skov, T. Krejsgaard, L. F. Bovin, M. L. Hansen, K. Grønbaek, N. Billestrup, M. H. Nissen, C. Geisler, et al. 2010. Deficient SOCS3 and SHP-1 expression in psoriatic T cells. *J. Invest. Dermatol.* 130: 1590–1597.
20. Christophi, G. P., M. Panos, C. A. Hudson, R. L. Christophi, R. C. Gruber, A. T. Mersich, S. D. Blystone, B. Jubelt, and P. T. Massa. 2009. Macrophages of multiple sclerosis patients display deficient SHP-1 expression and enhanced inflammatory phenotype. *Lab. Invest.* 89: 742–759.
21. Zhu, Z., S. Y. Oh, Y. S. Cho, L. Zhang, Y. K. Kim, and T. Zheng. 2010. Tyrosine phosphatase SHP-1 in allergic and anaphylactic inflammation. *Immunol. Res.* 47: 3–13.
22. Wu, C., M. Sun, L. Liu, and G. W. Zhou. 2003. The function of the protein tyrosine phosphatase SHP-1 in cancer. *Gene* 306: 1–12.
23. Witkiewicz, A., P. Raghunath, A. Wasik, J. M. Junkins-Hopkins, D. Jones, Q. Zhang, N. Odum, and M. A. Wasik. 2007. Loss of SHP-1 tyrosine phosphatase expression correlates with the advanced stages of cutaneous T-cell lymphoma. *Hum. Pathol.* 38: 462–467.
24. Dubois, M. J., S. Bergeron, H. J. Kim, L. Dombrowski, M. Perreault, B. Fournès, R. Faure, M. Olivier, N. Beauchemin, G. I. Shulman, et al. 2006. The SHP-1 protein tyrosine phosphatase negatively modulates glucose homeostasis. *Nat. Med.* 12: 549–556.
25. Geraldes, P., J. Hiraoka-Yamamoto, M. Matsumoto, A. Clermont, M. Leitges, A. Marette, L. P. Aiello, T. S. Kern, and G. L. King. 2009. Activation of PKC-delta and SHP-1 by hyperglycemia causes vascular cell apoptosis and diabetic retinopathy. *Nat. Med.* 15: 1298–1306.
26. Lieschke, G. J., and N. S. Trede. 2009. Fish immunology. *Curr. Biol.* 19: R678–R682.
27. Martin, J. S., and S. A. Renshaw. 2009. Using in vivo zebrafish models to understand the biochemical basis of neutrophilic respiratory disease. *Biochem. Soc. Trans.* 37: 830–837.
28. Meijer, A. H., and H. P. Spaink. 2011. Host-pathogen interactions made transparent with the zebrafish model. *Curr. Drug Targets* 12: 1000–1017.
29. Lam, S. H., H. L. Chua, Z. Gong, T. J. Lam, and Y. M. Sin. 2004. Development and maturation of the immune system in zebrafish, *Danio rerio*: a gene expression profiling, in situ hybridization and immunological study. *Dev. Comp. Immunol.* 28: 9–28.
30. van Eekelen, M., J. Overvoorde, C. van Rooijen, and J. den Hertog. 2010. Identification and expression of the family of classical protein-tyrosine phosphatases in zebrafish. *PLoS ONE* 5: e12573.
31. Zakrzewska, A., C. Cui, O. W. Stockhammer, E. L. Benard, H. P. Spaink, and A. H. Meijer. 2010. Macrophage-specific gene functions in Spi1-directed innate immunity. *Blood* 116: e1–e11.
32. Wlodarski, P., Q. Zhang, X. Liu, M. Kasprzycka, M. Marzec, and M. A. Wasik. 2007. PU.1 activates transcription of SHP-1 gene in hematopoietic cells. *J. Biol. Chem.* 282: 6316–6323.
33. Jopling, C., D. van Geemen, and J. den Hertog. 2007. Shp2 knockdown and Noonan/LEOPARD mutant Shp2-induced gastrulation defects. *PLoS Genet.* 3: e225.
34. Berghmans, S., R. D. Murphey, E. Wienholds, D. Neuberg, J. L. Kutok, C. D. Fletcher, J. P. Morris, T. X. Liu, S. Schulte-Merker, J. P. Kanki, et al. 2005. tp53 mutant zebrafish develop malignant peripheral nerve sheath tumors. *Proc. Natl. Acad. Sci. USA* 102: 407–412.
35. Renshaw, S. A., C. A. Loynes, D. M. Trushell, S. Elworthy, P. W. Ingham, and M. K. Whyte. 2006. A transgenic zebrafish model of neutrophilic inflammation. *Blood* 108: 3976–3978.
36. Lawson, N. D., and B. M. Weinstein. 2002. In vivo imaging of embryonic vascular development using transgenic zebrafish. *Dev. Biol.* 248: 307–318.
37. Liu, N. A., Q. Liu, K. Wawrowsky, Z. Yang, S. Lin, and S. Melmed. 2006. Prolactin receptor signaling mediates the osmotic response of embryonic zebrafish lactotrophs. *Mol. Endocrinol.* 20: 871–880.
38. Stockhammer, O. W., A. Zakrzewska, Z. Hegedûs, H. P. Spaink, and A. H. Meijer. 2009. Transcriptome profiling and functional analyses of the zebrafish embryonic innate immune response to *Salmonella* infection. *J. Immunol.* 182: 5641–5653.
39. Mathias, J. R., M. E. Dodd, K. B. Walters, J. Rhodes, J. P. Kanki, A. T. Look, and A. Huttenlocher. 2007. Live imaging of chronic inflammation caused by mutation of zebrafish Hai1. *J. Cell Sci.* 120: 3372–3383.
40. Cui, C., E. L. Benard, Z. Kanwal, O. W. Stockhammer, M. van der Vaart, A. Zakrzewska, H. P. Spaink, and A. H. Meijer. 2011. Infectious disease modeling and innate immune function in zebrafish embryos. *Methods Cell Biol.* 105: 273–308.
41. Rotman, J., W. van Gils, D. Butler, H. P. Spaink, and A. H. Meijer. 2011. Rapid screening of innate immune gene expression in zebrafish using reverse transcription - multiplex ligation-dependent probe amplification. *BMC Res Notes* 4: 196.
42. Pham, L. N., M. Kanther, I. Semova, and J. F. Rawls. 2008. Methods for generating and colonizing gnotobiotic zebrafish. *Nat. Protoc.* 3: 1862–1875.
43. d'Alençon, C. A., O. A. Peña, C. Wittmann, V. E. Gallardo, R. A. Jones, F. Loosli, U. Liebel, C. Grabher, and M. L. Allende. 2010. A high-throughput chemically induced inflammation assay in zebrafish. *BMC Biol.* 8: 151.

44. van der Sar, A. M., R. J. P. Musters, F. J. M. van Eeden, B. J. Appelmelk, C. M. J. E. Vandenbroucke-Grauls, and W. Bitter. 2003. Zebrafish embryos as a model host for the real time analysis of *Salmonella typhimurium* infections. *Cell. Microbiol.* 5: 601–611.
45. van der Sar, A. M., A. M. Abdallah, M. Sparrius, E. Reinders, C. M. Vandenbroucke-Grauls, and W. Bitter. 2004. *Mycobacterium* marinum strains can be divided into two distinct types based on genetic diversity and virulence. *Infect. Immun.* 72: 6306–6312.
46. Huang, W., B. T. Sherman, and R. A. Lempicki. 2009. Systematic and integrative analysis of large gene lists using DAVID bioinformatics resources. *Nat. Protoc.* 4: 44–57.
47. Stoop, E. J., T. Schipper, S. K. Huber, A. E. Nezhinsky, F. J. Verbeek, S. S. Gurcha, G. S. Besra, C. M. Vandenbroucke-Grauls, W. Bitter, and A. M. van der Sar. 2011. Zebrafish embryo screen for mycobacterial genes involved in the initiation of granuloma formation reveals a newly identified ESX-1 component. *Dis Model Mech* 4: 526–536.
48. Robu, M. E., J. D. Larson, A. Nasevicius, S. Beiraghi, C. Brenner, S. A. Farber, and S. C. Ekker. 2007. p53 activation by knockdown technologies. *PLoS Genet.* 3: e78.
49. Schaaf, M. J., A. Chatzopoulou, and H. P. Spaink. 2009. The zebrafish as a model system for glucocorticoid receptor research. *Comp. Biochem. Physiol. A Mol. Integr. Physiol.* 153: 75–82.
50. Schoonheim, P. J., A. Chatzopoulou, and M. J. Schaaf. 2010. The zebrafish as an in vivo model system for glucocorticoid resistance. *Steroids* 75: 918–925.
51. Davis, J. M., H. Clay, J. L. Lewis, N. Ghori, P. Herbomel, and L. Ramakrishnan. 2002. Real-time visualization of *mycobacterium*-macrophage interactions leading to initiation of granuloma formation in zebrafish embryos. *Immunity* 17: 693–702.
52. van der Sar, A. M., H. P. Spaink, A. Zakrzewska, W. Bitter, and A. H. Meijer. 2009. Specificity of the zebrafish host transcriptome response to acute and chronic mycobacterial infection and the role of innate and adaptive immune components. *Mol. Immunol.* 46: 2317–2332.
53. Ordas, A., Z. Hegedus, C. V. Henkel, O. W. Stockhammer, D. Butler, H. J. Jansen, P. Racz, M. Mink, H. P. Spaink, and A. H. Meijer. 2011. Deep sequencing of the innate immune transcriptomic response of zebrafish embryos to *Salmonella* infection. *Fish Shellfish Immunol.* 31: 716–724.
54. Kundu, S., K. Fan, M. Cao, D. J. Lindner, Z. J. Zhao, E. Borden, and T. Yi. 2010. Novel SHP-1 inhibitors tyrosine phosphatase inhibitor-1 and analogs with preclinical anti-tumor activities as tolerated oral agents. *J. Immunol.* 184: 6529–6536.
55. Van Zant, G., and L. Shultz. 1989. Hematologic abnormalities of the immunodeficient mouse mutant, viable motheaten (mev). *Exp. Hematol.* 17: 81–87.
56. Lutzner, M. A., and C. T. Hansen. 1976. Motheater: an immunodeficient mouse with markedly less ability to survive that the nude mouse in a germfree environment. *J. Immunol.* 116: 1496–1497.
57. Massa, P. T., S. Saha, C. Wu, and K. W. Jarosinski. 2000. Expression and function of the protein tyrosine phosphatase SHP-1 in oligodendrocytes. *Glia* 29: 376–385.
58. Horvat, A., F. Schwaiger, G. Hager, F. Brocker, R. Streif, P. Knyazev, A. Ullrich, and G. W. Kreutzberg. 2001. A novel role for protein tyrosine phosphatase shp1 in controlling glial activation in the normal and injured nervous system. *J. Neurosci.* 21: 865–874.
59. Barnes, P. J. 2006. Corticosteroids: the drugs to beat. *Eur. J. Pharmacol.* 533: 2–14.
60. De Bosscher, K., and G. Haegeman. 2009. Minireview: latest perspectives on antiinflammatory actions of glucocorticoids. *Mol. Endocrinol.* 23: 281–291.
61. Zhang, Z., S. Jones, J. S. Hagood, N. L. Fuentes, and G. M. Fuller. 1997. STAT3 acts as a co-activator of glucocorticoid receptor signaling. *J. Biol. Chem.* 272: 30607–30610.
62. Biola, A., K. Andréau, M. David, M. Sturm, M. Haake, J. Bertoglio, and M. Pallardy. 2000. The glucocorticoid receptor and STAT6 physically and functionally interact in T-lymphocytes. *FEBS Lett.* 487: 229–233.
63. Hermoso, M. A., T. Matsuguchi, K. Smoak, and J. A. Cidlowski. 2004. Glucocorticoids and tumor necrosis factor alpha cooperatively regulate toll-like receptor 2 gene expression. *Mol. Cell. Biol.* 24: 4743–4756.
64. Stoecklin, E., M. Wissler, R. Moriggl, and B. Groner. 1997. Specific DNA binding of Stat5, but not of glucocorticoid receptor, is required for their functional cooperation in the regulation of gene transcription. *Mol. Cell. Biol.* 17: 6708–6716.
65. Rogatsky, I., and L. B. Ivashkiv. 2006. Glucocorticoid modulation of cytokine signaling. *Tissue Antigens* 68: 1–12.
66. Engblom, D., J. W. Kornfeld, L. Schwake, F. Tronche, A. Reimann, H. Beug, L. Hennighausen, R. Moriggl, and G. Schütz. 2007. Direct glucocorticoid receptor-Stat5 interaction in hepatocytes controls body size and maturation-related gene expression. *Genes Dev.* 21: 1157–1162.
67. Valentino, L., and J. Pierre. 2006. JAK/STAT signal transduction: regulators and implication in hematological malignancies. *Biochem. Pharmacol.* 71: 713–721.
68. Barnes, P. J., and I. M. Adcock. 2009. Glucocorticoid resistance in inflammatory diseases. *Lancet* 373: 1905–1917.
69. Stockhammer, O. W., H. Rauwerda, F. R. Wittink, T. M. Breit, A. H. Meijer, and H. P. Spaink. 2010. Transcriptome analysis of Traf6 function in the innate immune response of zebrafish embryos. *Mol. Immunol.* 48: 179–190.
70. Gomez, M. A., I. Contreras, M. Hallé, M. L. Tremblay, R. W. McMaster, and M. Olivier. 2009. *Leishmania* GP63 alters host signaling through cleavage-activated protein tyrosine phosphatases. *Sci. Signal.* 2: ra58.
71. Knutson, K. L., Z. Hmama, P. Herrera-Velit, R. Rochford, and N. E. Reiner. 1998. Lipoarabinomannan of *Mycobacterium tuberculosis* promotes protein tyrosine dephosphorylation and inhibition of mitogen-activated protein kinase in human mononuclear phagocytes. Role of the Src homology 2 containing tyrosine phosphatase 1. *J. Biol. Chem.* 273: 645–652.
72. Rojas, M., M. Olivier, and L. F. García. 2002. Activation of JAK2/STAT1-alpha-dependent signaling events during *Mycobacterium tuberculosis*-induced macrophage apoptosis. *Cell. Immunol.* 217: 58–66.
73. Clay, H., H. E. Volkman, and L. Ramakrishnan. 2008. Tumor necrosis factor signaling mediates resistance to mycobacteria by inhibiting bacterial growth and macrophage death. *Immunity* 29: 283–294.
74. Tobin, D. M., J. C. Vary, Jr., J. P. Ray, G. S. Walsh, S. J. Dunstan, N. D. Bang, D. A. Hagge, S. Khadge, M. C. King, T. R. Hawn, et al. 2010. The lta4h locus modulates susceptibility to mycobacterial infection in zebrafish and humans. *Cell* 140: 717–730.
75. Tobin, D. M., F. J. Roca, S. F. Oh, R. McFarland, T. W. Vickery, J. P. Ray, D. C. Ko, Y. Zou, N. D. Bang, T. T. Chau, et al. 2012. Host genotype-specific therapies can optimize the inflammatory response to mycobacterial infections. *Cell* 148: 434–446.